Table 1 Clinical characteristics in the patients with GBMO ($n = 19$)

Age	24–75 years old (median 58, average 53)					
Gender	Male/female = 13/6					
Location	Frontal lobe	:	5	Temporal lobe	:	7
	Parietal lobe	:	4	Posterior lobe	:	1
	Basal ganglia	:	2			
Radiological findings	Calcification	:	11	Cyst	:	9
Removal	Gross total removal	:	11			
	Partial removal	:	8			
Radiotherapy	Extended local[a] 40 Gy + local 20 Gy	:	18			
	Stereotactic radiosurgery	:	1			
Chemotherapy	ACNU or TMZ	:	17	None	:	2

GBMO glioblastoma with oligodendroglial component, *ACNU* nimustine, *TMZ* temozolomide

[a] Radiation area covering a 2 cm margin of MRI T2-weighted high-intensity area

to extract DNA. To obtain a histopathological diagnosis, we stained sections from paraffin-embedded tumor blocks with hematoxylin and eosin (H&E). DNA was extracted from frozen tumor tissue and blood samples for single nucleotide polymorphism (SNP) oligonucleotide genomic microarray analysis [9]. Briefly, first genomic DNA from tumor and blood samples was restriction enzyme-digested, and the adaptor was ligated at both termini. This was followed by PCR amplification using primers that recognize the adaptor site. The PCR products were hybridized and analyzed using a gene chip mapping array and CNAG software. This method facilitated the detection of whole-genome alterations. We looked for loss of heterozygosity (LOH) of chromosomes 1p, 9p, 10, 17p (p53 locus), and 19q, and for the gene amplification of EGFR and PDGFRA. All statistical analyses were with STATMATE software. Overall survival (OS) was defined as the interval between surgery and death. Survival curves were obtained using the Kaplan–Meier method.

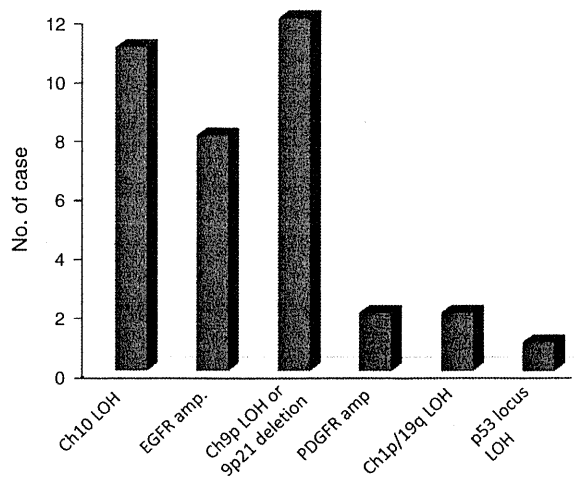

Fig. 1 *Bar graph* of the number of genetic alterations. Chromosome 10 LOH, EGFR amplification, and homozygous deletion of 9p21 were frequently seen

Results

The median age of the 19 GBMO patients (13 men and 6 women) was 58 years (range 24–75 years). The tumor was located in the frontal lobe in 5, the temporal lobe in 7, the parietal lobe in 4, the occipital lobe in 1, and the basal ganglia in 2 patients. Radiological studies revealed that 9 tumors harbored cysts and 11 contained areas of calcification. All patients underwent gross total ($n = 11$) or partial tumor resection ($n = 8$), and all received radiotherapy. A chemotherapy regimen of ACNU or TMZ was used in 17 patients; 2 did not undergo chemotherapy.

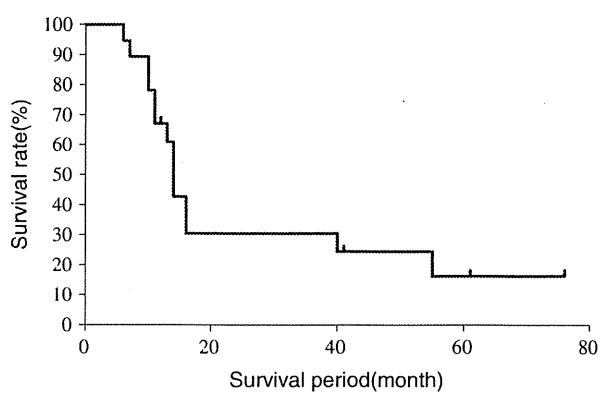

Fig. 2 Kaplan–Meier survival curve of patients with GBMO

Molecular analysis using SNP microarrays

As shown in Fig. 1, in our 19 patients we documented LOH of chromosome 10 ($n = 11$, 58%), EGFR amplification ($n = 8$, 42%), LOH of chromosome 9 or a homozygous deletion in 9p21 (INK4A locus) ($n = 12$, 63%), PDGFRA amplification ($n = 2$, 11%), LOH of chromosome 1p or

19q ($n = 2$ each, 11%), and LOH of chromosome 17p (p53 locus) ($n = 1$, 5%).

Survival

Median OS was 14 months (average 22.8 months). The Kaplan–Meier survival curve is presented in Fig. 2. Survival in our series of 19 GBMO patients was similar to that of GBM patients treated at our institution.

Illustrative cases

Case 1

This 51-year-old man presented with headache in July 2006. MRI revealed an irregularly enhanced tumor containing a cyst in his left frontal lobe; CT showed an area of calcification within the tumor (Fig. 3a, b). The tumor was removed completely. Pathological findings indicated that the tumor tissue contained an area with typical clear cells (honeycomb appearance); the presence of a partially necrotic area with endothelial proliferation was also confirmed (Fig. 3c–e). SNP microarray analysis revealed PDGFRA amplification (Fig. 3f) and LOH of chromosome 10 (Fig. 3h). Chromosome 9 was intact (Fig. 3g). There was no LOH of chromosome 1p/19q. This pattern of genetic alterations was reminiscent of the pattern often seen in GBM. Postoperatively the patient received chemotherapy and concomitant radiotherapy, and he was discharged with no neurological deficits.

Case 2

This 31-year-old woman presented in May 2009 with mild paresthesia of her right hand. MRI revealed a tumor containing a cyst in her left parietal lobe, and a CT scan showed a small calcification in the tumor (Fig. 4a, b). Pathological study of the partially removed tumor detected oligodendroglioma-like cells and a necrotic area (Fig. 4c–f), and a diagnosis of GBMO was made. SNP microarray analysis revealed EGFR amplification (Fig. 4g), LOH of chromosome 10 (Fig. 4i), and a homozygous deletion in

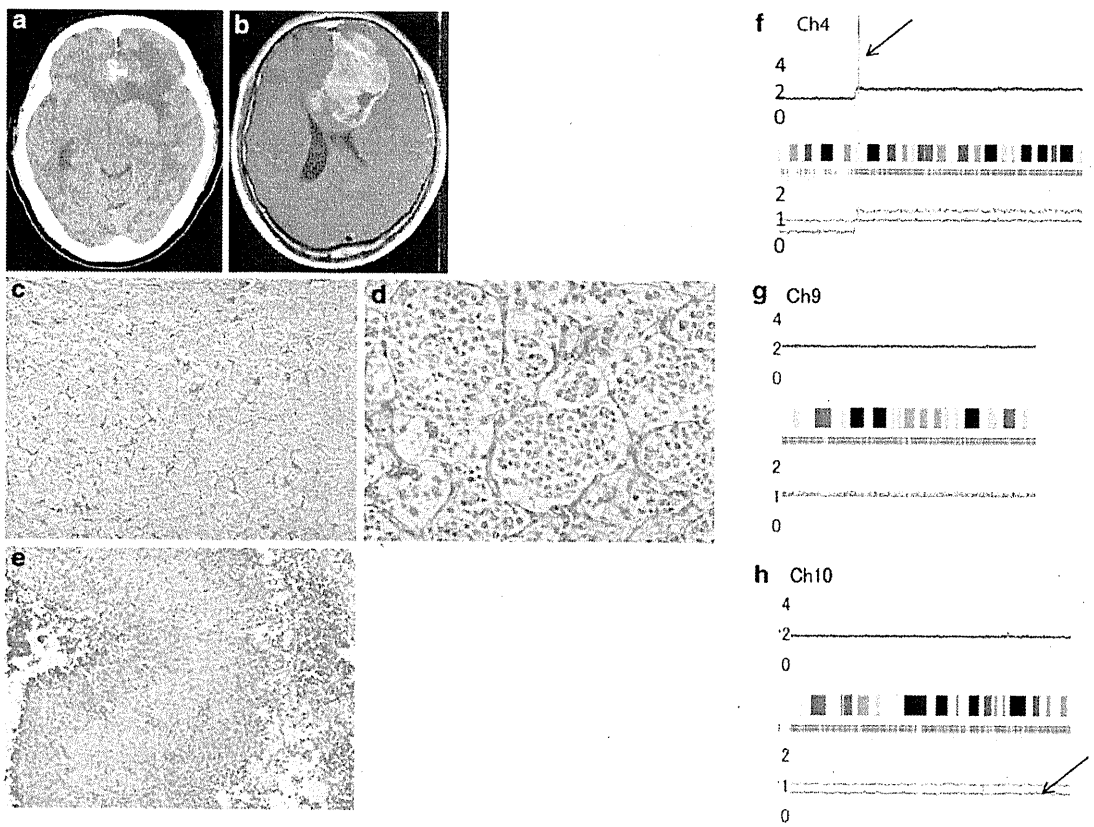

Fig. 3 Illustrative case 1. **a** CT scan revealing a tumor in the left frontal lobe. Calcification and perifocal edema were observed. **b** The gadolinium-enhanced tumor was located in the left frontal lobe; it compressed the left lateral ventricle. **c** H&E staining demonstrated clear cells as are seen in oligodendroglioma (×10). **d** High magnification of **c** (×40). **e** In the tumor we observed partially necrotic tissue and endothelial proliferation (×10). **f** SNP microarray analysis of chromosome 4 revealed PDGFRA amplification (*arrow*). **g** Chromosome 9 was intact. **h** There was LOH of chromosome 10 (*arrow*)

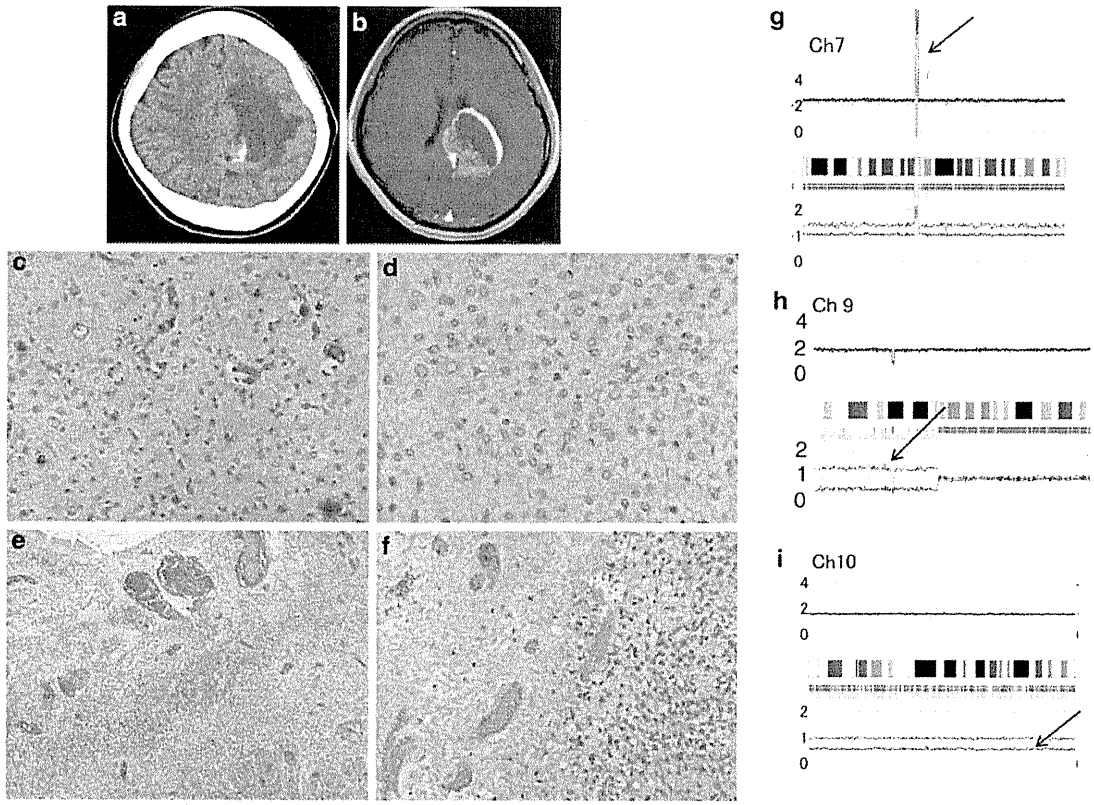

Fig. 4 Illustrative case 2. **a** CT scan revealing a tumor in the left parietal lobe. Calcification, cyst, and perifocal edema were observed. **b** The gadolinium-enhanced tumor was located in the left parietal lobe. **c** H&E staining demonstrated calcification and oligodendroglioma-like tumor cells (×10). **d** High magnification of **c** (×40). **e** In the tumor we noted partial hemorrhage, necrotic tissue, and endothelial proliferation (×5). **f** Necrotic tissue was observed (×10). **g** SNP microarray analysis of chromosome 7 revealed EGFR amplification (*arrow*). **h** There was a homozygous deletion in 9p21. **i** There was LOH of chromosome 10 (*arrow*)

chromosome 9p21 (INK4A locus) (Fig. 4h). There was no LOH of chromosome 1p/19q. The patient underwent chemo- and radiotherapy, and is doing well 2 years after surgery.

Discussion

In the 2007 WHO classification, anaplastic oligoastrocytoma with necrosis is defined as glioblastoma with oligodendroglial components (GBMO) [5]. However, definite diagnostic criteria for this entity have not been determined, and the clinical outcome of GBMO patients remains controversial. Some reported that the prognosis was better in GBMO than in GBM patients [7, 10], whereas others claimed that the prognosis of these patients was similar.

Using SNP microarray analysis to genetically characterize GBMOs that had been diagnosed pathologically, we obtained information on genomic alterations and compared the observed alteration patterns in whole chromosomes. According to Kraus et al. [11], in patients with GBM, LOH of chromosome 10 and EGFR is frequent, whereas LOH of chromosome 1p/19q is rare. Cairncross et al. [12] reported a high incidence of LOH of chromosome 1p/19q in patients with anaplastic oligodendroglioma. The pattern of genetic alterations in our GBMO patients was similar to patterns seen in patients with GBM.

In 2008, Parsons et al. [13] first reported a mutation in the isocitrate dehydrogenase (IDH-1) gene in patients with glioma. Subsequently, it was demonstrated that the IDH-1 gene was most commonly mutated in grade II and III gliomas and in secondary types of GBM, but not in de novo GBM, and that patients with IDH-1 mutations survived longer than patients without [14–16]. We looked for IDH-1 mutations in some of our patients but were unable to find such mutations (data not shown). The median OS of our patients was 14 months (average 22.8 months) and similar to that of patients with typical GBM. Based on our findings we posit that the biological features of the tumors in our series were more like those of GBM than of anaplastic oligoastrocytoma. Although GBMO is pathologically defined as anaplastic oligoastrocytoma with necrosis, we

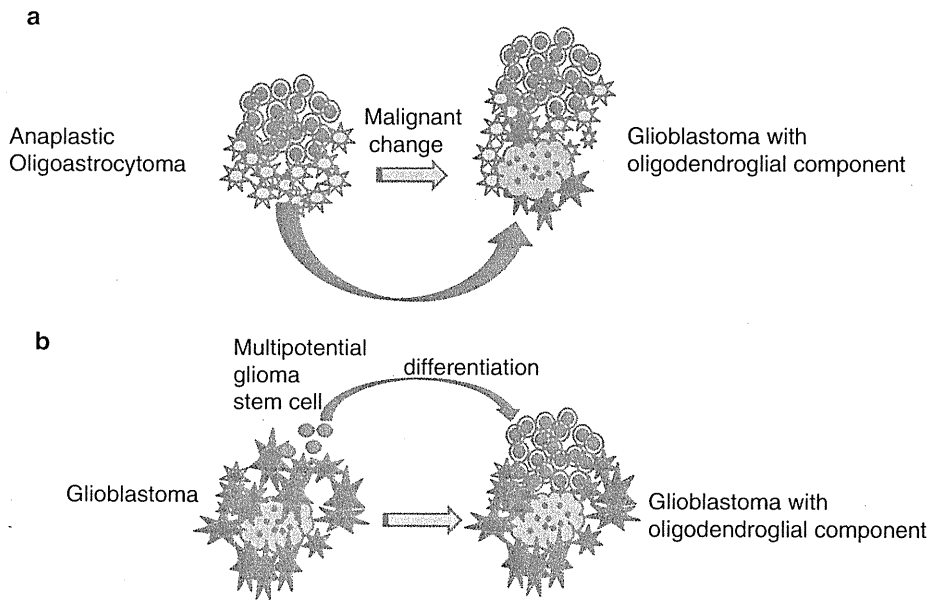

Fig. 5 Schema of our hypothesis on the induction of GBMO. **a** Within anaplastic oligoastrocytoma some tumor cells exhibit malignant transformation; some necrotic tissue is present. **b** Some tumor cells within GBM (especially multipotent glioma stem cells) differentiated into oligodendroglioma-like cells

suggest that two possible pathways may lead to the induction of GBMO (Fig. 5). Under one scenario, some cells in the anaplastic oligoastrocytoma cell population, particularly astrocytoma cells, may undergo malignant transformation. According to several reports about the molecular profile in gliomas, 1p19q LOH seems to be found in 40–60% of the patients with anaplastic oligoastrocytoma. However, in this study of molecular analysis, 1p19q LOH was seen in only two patients (11%), which seems to be relatively low. Under the other scenario, some among the GBM cells, e.g., multi-potent glioma stem cells, may differentiate to oligodendroglioma-like tumor cells.

In this study we suggest the latter scenario is reasonable.

Conclusion

The pattern of genetic alterations is similar in GBMO and GBM patients, and the clinical outcomes in these patients are also similar.

Acknowledgments The authors thank Seishi Ogawa for assistance with the SNP microarray analysis and Masayo Obata for help with the pathological techniques.

References

1. Homma T, Fukushima T, Vaccarella S et al (2006) Correlation among pathology, genotype, and patient outcomes in glioblastoma. J Neuropathol Exp Neurol 65:846–854
2. Hilton DA, Penney M, Pobereskin L et al (2004) Histological indicators of prognosis in glioblastomas: retinoblastoma protein expression and oligodendroglial differentiation indicate improved survival. Histopathology 44:555–560
3. Kraus JA, Lamszus K, Glesmann N et al (2001) Molecular genetic alterations in glioblastomas with oligodendroglial component. Acta Neuropathol 101:311–320
4. Miller CR, Perry A (2007) Glioblastoma. Arch Pathol Lab Med 131:397–406
5. Kleihues P, Burger KD, Aldape DJ et al (2007) Glioblastoma. In: WHO Classification for Tumors of the Central Nervous System. International Agency for Research on Cancer (IARC) Press, Lyon, pp 33–49
6. Cancer Genome Atlas Research Network (2008) Comprehensive genomic characterization defines human glioblastoma genes and core pathways. Nature 455:1061–1068
7. Salvati M, Formichella AI, D'Elia A et al (2009) Cerebral glioblastoma with oligodendrogliomal component: analysis of 36 cases. J Neurooncol 94:129–134
8. Klink B, Schlingelhof B, Klink M et al (2010) Glioblastomas with oligodendroglial component—common origin of the different histological parts and genetic subclassification. Anal Cell Pathol (Amst) 33:37–54
9. Kawamata N, Ogawa S, Zimmermann M et al (2008) Molecular allelokaryotyping of pediatric acute lymphoblastic leukemias by high-resolution single nucleotide polymorphism oligonucleotide genomic microarray. Blood 111:776–784
10. Vordermark D, Ruprecht K, Rieckmann P et al (2006) Glioblastoma multiforme with oligodendroglial component (GBMO): favorable outcome after post-operative radiotherapy and chemotherapy with nimustine (ACNU) and teniposide (VM 26). BMC Cancer 6:247
11. Kraus JA, Glesmann N, Beck M et al (2000) Molecular analysis of the PTEN, TP53 and CDKN2A tumor suppressor genes in long-term survivors of glioblastoma multiforme. J Neurooncol 48:89–94
12. Cairncross JG, Ueki K, Zlatescu MC et al (1998) Specific genetic predictors of chemotherapeutic response and survival in patients

with anaplastic oligodendrogliomas. J Natl Cancer Inst 90:1473–1479
13. Parsons DW, Jones S, Zhang X et al (2008) An integrated genomic analysis of human glioblastoma multiforme. Science 321:1807–1812
14. Watanabe T, Nobusawa S, Kleihues P et al (2009) IDH1 mutations are early events in the development of astrocytomas and oligodendrogliomas. Am J Pathol 174:1149–1153
15. Ichimura K, Pearson DM, Kocialkowski S et al (2009) IDH1 mutations are present in the majority of common adult gliomas but rare in primary glioblastomas. Neuro Oncol 11:341–347
16. Nobusawa S, Watanabe T, Kleihues P et al (2009) IDH1 mutations as molecular signature and predictive factor of secondary glioblastomas. Clin Cancer Res 15:6002–6007

Cancer Science
The official journal of the Japanese Cancer Association JCA

Essential role of the Hedgehog signaling pathway in human glioma-initiating cells

Tatsuya Takezaki,[1,2] Takuichiro Hide,[1,2] Hiromi Takanaga,[1] Hideo Nakamura,[2] Jun-ichi Kuratsu[2] and Toru Kondo[1,3,4]

[1]Laboratory for Cell Lineage Modulation, RIKEN Center for Developmental Biology, Kobe; [2]Department of Neurosurgery, Kumamoto University Graduate School of Medicine, Kumamoto; [3]Department of Stem Cell Biology, Ehime University Proteo-Medicine Research Center, To-on, Ehime, Japan

(Received January 18, 2011/Revised March 23, 2011/Accepted March 24, 2011/Accepted manuscript online March 31, 2011/Article first published online May 3, 2011)

Recent findings have demonstrated that malignant tumors, including glioblastoma multiforme, contain cancer-initiating cells (also known as cancer stem cells), which self-renew and are malignant, with features of tissue-specific stem cells. As these cells are resistant to irradiation and anti-cancer drugs, it is important to characterize them and find targeting therapies. In this study, we established two primary human glioma cell lines from anaplastic oligodendroglioma and glioblastoma multiforme. These lines were enriched in glioma-initiating cells, as just 10 cells formed malignant glioma when injected into mouse brain. We used these cell lines to examine the roles of the Notch, Hedgehog and Wnt signaling pathways, which are involved in stem-cell maintenance and tumorigenesis, to determine which of these pathways are crucial to glioma-initiating cells and their regulation. Here we show that the Hedgehog pathway is indispensable for glioma-initiating cell proliferation and tumorigenesis; the Hedgehog signaling inhibitors prevented glioma-initiating cell proliferation, while signaling inhibitors for Notch or Wnt did not. Overexpression of Gli2ΔC, a C-terminal-truncated form of Gli2 that antagonizes Gli transcription factor functions, blocked glioma-initiating cell proliferation in culture and tumorigenesis *in vivo*. Knockdown of the Gli downstream factor Cdc2 also prevented glioma-initiating cell proliferation. Taken together, these results show that the Hedgehog → Gli → Cdc2 signaling cascade plays a role in the proliferation and malignancy of glioma-initiating cells. (*Cancer Sci* 2011; 102: 1306–1312)

Cancer-initiating cells (CIC) are capable of indefinite self-renewal and generate the amplifying cancer cells that make up the majority of cells in a tumor.[1–4] The CIC-enriched cell populations can be obtained from various types of cancers including glioma, and from cancer cell lines with characteristics in common with tissue-specific stem cells such as side population cells, cell-surface antigens such as CD133, floating sphere formation or a combination of these features.[2–4] However, CIC and their specific markers and targets are not well characterized.

There are several lines of evidence that glioma cells and normal neural stem cells (NSC) share many mechanisms, including signaling pathways activated by Notch, Wnt and Hedgehog (Hh).[1,5] Notch signaling is strongly activated in both primary human gliomas and in many glioma cell lines.[6] Depleting Notch1 or the Notch ligands delta like 1 and Jagged1 by RNAi blocks glioma cell proliferation *in vivo* and *in vitro*.[7]

Ectopically activated Hh signaling in the central nervous system (CNS) causes brain tumors to form.[8,9] Gli1, a Hh-signaling effector molecule, is highly activated in many brain cancers[8] including glioblastoma multiforme (GBM). Overexpressing Gli1 in the developing tadpole CNS induces brain tumors,[10] whereas cyclopamine, which specifically inhibits Hh signaling, blocks the growth of primary gliomas and glioma cell lines.[10,11]

Finally, the canonical Wnt signaling pathway is involved in gliomagenesis; one of its essential mediators, β-catenin, is upregulated along with Wnt2 and Wnt5a in human gliomas and glioma cell lines. Overexpressing a stabilized form of β-catenin in NSC causes lateral ventricle hyperplasia,[12] whereas β-catenin knockdown inhibits glioma cell proliferation *in vitro* and *in vivo*.[13,14]

The Notch, Hh and Wnt signaling pathways all appear to be important for gliomagenesis, but it is uncertain whether they are equally essential for the proliferation and maintenance of the glioma-initiating cell (GIC). Using human GIC lines established from anaplastic oligodendroglioma (AO) and GBM, we show that the Hh signaling cascade Hh → Gli → Cdc2 is indispensable for GIC proliferation and malignancy, whereas inhibiting either the Notch or Wnt signaling pathway has little effect.

Materials and Methods

Animals and chemicals. Mice were obtained from Charles River Japan, Inc. (Yokohama, Japan). All mouse experimental protocols were approved by the RIKEN Center for Developmental Biology Animal Care and Use Committee. Chemicals and growth factors were purchased from Sigma (St. Louis, MO, USA) and Peprotech (Rocky Hill, NJ, USA), respectively, except where indicated.

Primary human glioma cell culture and human brain tumors. Two primary human glioma samples, AO and GBM, were obtained at Kumamoto University Hospital with patients' consent, according to the Research Ethics Committee guidelines. Tumor samples were washed twice with PBS and dissociated with an enzymatic solution containing 0.25% Trypsin in 0.1 mM EDTA at 37°C for 60 min. Dissociated cells were then cultured as tumor spheres in serum-free NeuroBasal Medium-A (Gibco, Invitrogen, Carlsbad, CA, USA) containing human basic fibroblast growth factor (bFGF; 20 μM), human epidermal growth factor (EGF; 20 μM), human leukemia inhibitory factor (LIF, 20 μM; Chemicon, Millipore, Billerica, MA, USA), heparin (5 μM), insulin (10 μM), N2 supplement (1%, Gibco), B27 supplement (1%, Gibco) and GlutaMAX1 (Gibco) (NSC medium). The GIC were cultured on poly-D-lysine (PDL; 15 μg/mL)- and fibronectin (1 μg/mL)-coated eight-well chamber slides (Nunc) for immunostaining. To assess GIC multipotentiality, the cells were cultured in DMEM/F12 (Gibco) with 1% fetal calf serum alone (differentiation medium) for 2 days. Two GIC and four GBM were used in accordance with the research guidelines of the RIKEN CDB and the Kumamoto University Graduate School of Medical Science.

Intracranial cell transplantation into the brain of nude mice. The GIC were suspended in 5 μL of culture medium and injected into the brain of 5- to 8-week-old female nude mice, as described previously.[15]

Mouse brain fixation and histopathology. Mouse brains were dissected and fixed in 4% paraformaldehyde overnight,

[4]To whom correspondence should be addressed.
E-mail: tkondo@m.ehime-u.ac.jp

doi: 10.1111/j.1349-7006.2011.01943.x

transferred to 70% ethanol, processed on Tissue-Tek VIP (Sakura Finetek Japan, Tokyo, Japan) and embedded in paraffin. Coronal sections (6 μm thick) from the cerebral cortex were prepared on a Microtome and stained with hematoxylin–eosin (HE).

Immunostaining. Immunostaining was carried out as previously described.[16,17] The following antibodies were used to detect antigens: rabbit anti-CD133 (1:200; Abcam, Cambridge, MA, USA), mouse anti-Nestin (1:200; Chemicon), mouse anti-beta tubulin isotype III (βIII tubulin) (1:200; Sigma), rabbit anti-glial fibrillary acidic protein (GFAP) (1:400; Dako, Copenhagen, Denmark), rat anti-galactocerebroside (GC) (1:4; hybridoma supernatant; ATCC, Manassas, VA, USA) and rat anti-green fluorescent protein (GFP) (1:400; Nacalai Tesque, Kyoto, Japan). Antibodies were detected with goat anti-rat IgG-Alexa488 (1:400; Molecular Probes, Eugene, OR, USA), goat anti-rabbit IgG-Cy3 (1:400; Jackson ImmunoResearch, West Grove, PA, USA) and goat anti-mouse IgG-Alexa488 (1:400; Molecular Probes). The cells were counterstained with DAPI (1 μg/mL) to label the nuclei.

Paraffin-embedded tumors were sectioned at 6 μm thickness and immunostained as previously described.[15] The following antibodies were used to detect antigens: mouse monoclonal anti-Bmi1 (1:200; Abcam), mouse monoclonal anti-Notch (1:200; Abcam), rabbit polyclonal anti-Hes1 (1:200; Santa Cruz Biotechnology, Santa Cruz, CA, USA), rabbit polyclonal anti-Hes5 (1:200; Chemicon), rabbit polyclonal anti-β-catenin (1:200; Abcam), rabbit anti-Sox2 (1:500; StemCell Technologies, Vancouver, BC, Canada), guinea pig anti-Gli2 (1:100),[16] mouse anti N-myc (1:200; Calbiochem, Merck, Darmstadt, Germany) and mouse anti-Cdc2 (1:500; Abcam).

For TUNEL assays, the *In Situ* Cell Death Detection Kit, TMR red was used according to the supplier's instructions (Roche, Basel, Switzerland).

RT-PCR. Total RNA was prepared with the RNeasy mini kit (Qiagen, Hilden, Germany), the cDNA was synthesized with the Transcription First Strand cDNA Synthesis kit (Roche) and RT-PCR was carried out as previously described.[16,17] Primer sequences are provided in Table S1.

Vector construction. Vector construction was carried out as previously described.[15,16] In brief, full-length human sox2, bmi1, n-myc and cdc2 were amplified from human fetal brain cDNA libraries (Clontech, Mountain View, CA, USA) using RT-PCR and KOD plus DNA polymerase ver.2 (Toyobo, Osaka, Japan) according to the manufacturer's instructions, and were cloned into a pMOSBlue vector (GE Healthcare, Little Chalfont, UK). To construct the FLAG-tagged expression vector, cDNA was inserted into a p3xFLAG-CMV10 vector (Sigma) (FLAG-cont), resulting in p3xFLAG-sox2 (FLAG-Sox2), p3xFLAG-bmi1 (FLAG-Bmi1), p3xFLAG-n-myc (FLAG-Nmyc) and p3xFLAG-cdc2 (FLAG-Cdc2). Primer sequences for cDNA amplication are provided in Table S2.

To construct a tetracycline-dependent Gli2ΔC expression vector, Gli2ΔC cDNA was inserted into a pTRE2-hyg vector (Clontech), producing pTRE2-hyg-Gli2ΔC.

To knockdown human *bmi1*, *n-myc*, *sox2* and *cdc2*, their hairpin sequences were inserted into a psiRNA-h7SKhygro G1 expression vector (InvivoGen, San Diego, CA, USA), producing psiRNA-h7SKhygro-bmi1sh, psiRNA-h7SKhygro-nmycsh, psiRNA-h7SKhygro-sox2sh and psiRNA-h7SKhygro-cdc2sh, respectively. The siRNA target sequences for human *n-myc*, *sox2* and *cdc2* were 5′-GAAGAAATCGACGTGGTCACT-3′, 5′-GAAGGAGCACCCGGATTATAA-3′, and 5′-GAATCTTTACAGGACTATA-3′, respectively. The siRNA target sequence for *bmi1* was kindly provided by Dr Maarten van Lohuizen of The Netherlands Cancer Institute (Amsterdam, The Netherlands).

Transfection. Transfection was performed as described previously.[15,16] In brief, the cells were transfected with the vector using the Nucleofector device (Lonza, Cologne, Germany) according to the supplier's instructions, and were cultured for 24 h, after which the GFP-positive cells were collected by JSAN flow cytometry (Bay Bioscience, Kobe, Japan) and immunostained as described above.

For shRNA experiments, transfected cells were selected in an optimized medium with Hygromycin-B (1 mg/mL; Wako Chemical, Osaka, Japan) for 10 days. Stable hygromycin-resistant clones, of which there were more than 50, were mixed and used for experiments.

To establish inducible Gli2ΔC-bearing GIC lines, GIC were transfected with pTet-On vector (Clonetech) as described above, and selected with G418 sulfate (1 mg/mL; Nacalai Tesque). The G418-resistant GIC were then transfected with the pTRE2-hyg-Gli2ΔC vector and selected with Hygromycin-B. Inducible Gli2ΔC-bearing GIC clones were established by limiting dilution assays, and their proliferation was assayed in the presence

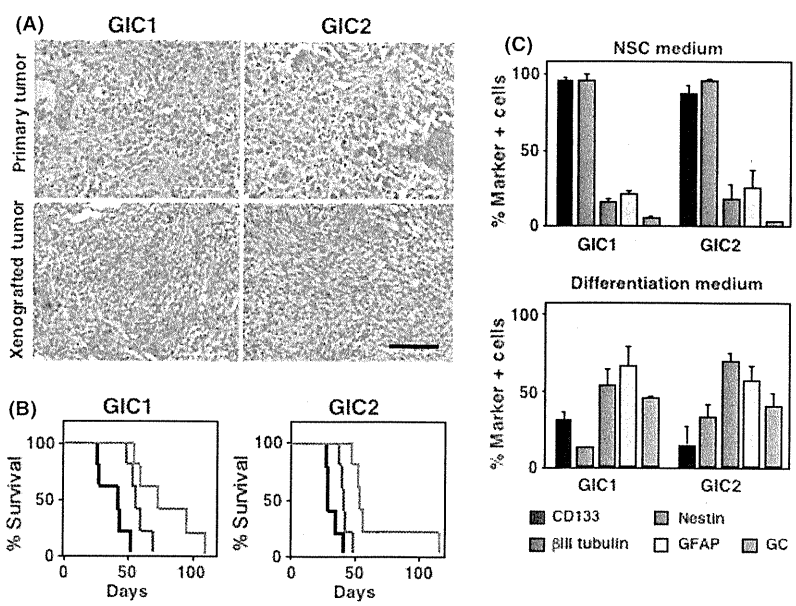

Fig. 1. Characterization of human glioma-initiating cells (GIC). (A) Tumors stained with hematoxylin–eosin (upper panels, primary tumors; lower panels, xenografts) displayed typical histopathological features of malignant glioma. Scale bar, 100 μm. (B) Survival curves for mice injected with a limiting dilution (black line, 1000; blue line, 100; red line, 10) of GIC1- or GIC2-injected mice ($n = 5$). (C) Immunocytochemical analysis of GIC for CD133, Nestin, βIII-tubulin, glial fibrillary acidic protein (GFAP) and galactocerebroside (GC). NSC, neural stem cells.

of Doxycycline hyclate (Dox, Clontech). The selected clones were transplanted into the brain of nude mice, and tumorigenesis was examined by daily intraperitoneal Dox injection (100 μL of 150 μg/mL) for up to 30 days.

Cell proliferation assay. To examine cell proliferation, MTT assays were performed as described previously.[15,16] Various concentrations of γ-Secretase Inhibitor (Calbiochem), Cyclopamine (Toronto Research Chemicals, Toronto, Canada) and Wnt inhibitor (WIF-1) (R&D Systems, Minneapolis, MN, USA) were added to the medium to examine the effects of blockading the Notch, Hh and Wnt signaling pathways, respectively.

Statistical analysis. Survival data were analyzed for significance using Kaplan–Meier methods with GraphPad Prism version 5 software (*P*-values were calculated with the Log-rank test).

Results

Characterization of human GIC lines. We established two human GIC lines, GIC1 and GIC2, from AO and GBM, respectively, as described previously.[18,19] Both GIC lines formed floating spheres in NSC medium and could be expanded and maintained thereafter.

We first examined the tumor-forming ability of each GIC line *in vivo* by injecting 10^3 cells into the brain of nude mice. All mice (n = 5 for each cell line) transplanted with GIC1 or GIC2 developed malignant glioma with hypercellularity, nuclear pleomorphism, mitosis, microvascular proliferation, hemorrhage and necrosis (Fig. 1A) and died within 53 or 42 days, respectively (Fig. 1B). Detailed histopathological examination revealed that GIC1-derived tumor was composed of a dense population of mitotically active cells with rounded, hyperchromatic nuclei and abundant microcysts, while GIC2 formed hypercellular tumors composed of mixed large and small anaplastic cells, consistent with their original pathological features. We then evaluated the frequency of GIC in these lines. All mice (n = 5 each) injected with 100 and 10 GIC1 cells died within 70 and 108 days, respectively, while all mice (n = 5 each) injected with 100 and 10 GIC2 cells died within 49 and 118 days, respectively (Fig. 1B). Using limiting dilution assays we further found that 15 of 24 single clones of GIC1 and 19 of 24 single clones of GIC2 were expandable in culture and formed colonies in soft agar. In addition, all of 10 GIC sublines, which were picked up randomly, retained their tumorigenicity *in vivo* (data not shown), suggesting that our GIC lines are enriched in GIC.

To characterize these GIC lines further, we immunolabeled them for NSC markers CD133 and Nestin, and for the neuronal, astrocyte and oligodendrocyte differentiation markers βIII tubulin, glial fibrillary acidic protein (GFAP) and galactocerebroside (GC). Both GIC lines prominently expressed the NSC markers, and only a small number of cells were positive for differentiation markers in NSC medium (Fig. 1C). In contrast, when the cells were cultured in differentiation medium for 2 days, they lost their NSC marker expression and expressed differentiation markers. As GIC1 was established from AO, we examined whether GIC1 predominantly expresses mature oligodendrocyte markers, myelin basic protein and glutathione S-transferase-pi in the presence of the inducers, IGF1 and thyroid hormone,[20] compared with GIC2. However, we could not find such a tendency (data not shown). Together, these data suggest that both GIC lines are multipotent.

Notch, Hh, Wnt and other NSC-related signaling factors are expressed in GIC. We used RT-PCR to determine whether NSC-related genes, including genes involved in the Notch, Hh and Wnt signaling pathways, are expressed in GIC. As shown in Figure 2A, both GIC1 and GIC2 expressed a number of these genes, although GIC2 did not express *wnt3a*, *wnt5a* or *wnt10b*, and neither GIC line expressed *sox1* nor *jagged (jag) 1*. We could not detect the expression of *jag2*, *deltex* (*dtx*) *1-4*, *wnt4*, *wnt7*, *wnt8*, *wnt11*, *wnt receptor frizzled homolog* (*fzd*) *2*, *fzd4*, *fzd5*, *fzd8*, *secreted frizzled-related protein* (*sfrp*) *1*; *sfrp2*, *sfrp4*, *wnt inhibitory factor* (*wif*), *seven-in-absentia* (*siah*) *1 and 2* or *norrin* in either GIC line (data not shown). We confirmed the expression of Sox2, Bmi1, Gli2, N-myc, Notch1, Hes1, Hes5 and β-catenin in the paraffin-embedded GIC xenografts by immunohistochemical analysis (Fig. 2B). These data suggest that GIC hijack the molecular machineries that work in NSC.

The Hh signaling pathway is indispensable for GIC proliferation, survival and tumorigenesis. While there is much evidence that Notch, Wnt and Hh are all involved in gliomagenesis,[1,5] it is not clear which of these signaling pathways are essential for GIC proliferation and malignancy. To address this question, we examined the effect of a γ-secretase inhibitor, cyclopamine, and Wnt inhibitory factor 1 (WIF1), which

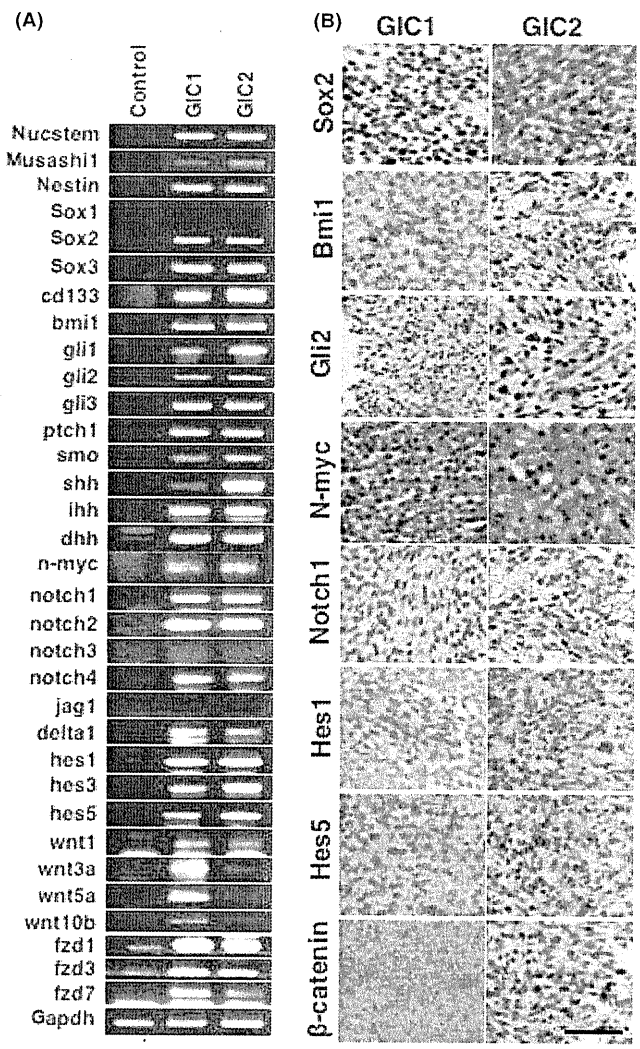

Fig. 2. Glioma-initiating cell (GIC) express factors involved in neural stem cell (NSC) proliferation and maintenance. (A) The expression of selected genes involved in NSC proliferation and maintenance was examined by RT-PCR. *gapdh* expression is an internal control. (B) Immunohistochemical analysis for the NSC markers Sox2, Bmi1, Gli2, N-myc, Notch1, Hes1, Hes5 and β-catenin on paraffin-embedded primary human glioblastoma multiforme (GBM) tissues. Scale bar, 50 μm.

doi: 10.1111/j.1349-7006.2011.01943.x

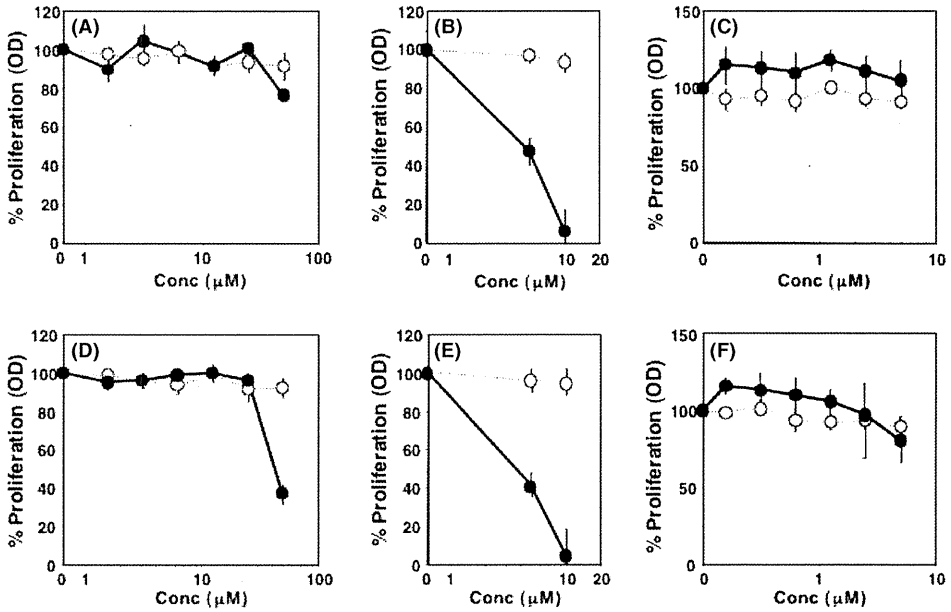

Fig. 3. Effects of Notch, Hedgehog (Hh) and Wnt inhibitors on glioma-initiating cell (GIC) proliferation. GIC1 (A–C) and GIC2 (D–F) cell proliferation in the absence (open circles) and presence (closed circles) of γ-secretase inhibitor (A,D), cyclopamine (B,E) or WIF1 (C,F) was examined by MTT assay.

specifically block the Notch, Hh and Wnt signaling pathways, respectively, in GIC. We found that cyclopamine strongly prevented cell proliferation in both GIC lines, whereas WIF1 or the γ-secretase inhibitor did not (Fig. 3). We confirmed that other Hh signaling inhibitors, JK418, Jervine, SANT1 and U18666A (Data S1) could block GIC proliferation (Fig. S1).

To verify that the Hh pathway is critical for GIC proliferation, we constructed a truncated form of Gli2 (Gli2ΔC) that antagonizes the functions of all three Gli transcription factors, overexpressed it in the cells and examined their proliferation. We found that Gli2ΔC overexpression prevented both GIC lines from proliferating and induced their death, just as it does in NSC[16] (Fig. 4).

We then examined whether Gli2ΔC overexpression prevents GIC tumorigenesis *in vivo*. Because overexpressing Gli2ΔC induced cell cycle arrest and apoptosis, we established the tetracycline (Tet)-inducible Gli2ΔC-expressing GIC lines Tet-On/Gli2ΔC-GIC1 and Tet-On/Gli2ΔC-GIC2. We confirmed that Tet-On/Gli2ΔC-GIC proliferation was blocked by the presence of Dox in culture (Fig. 5A). We then transplanted Tet-On/Gli2ΔC-GIC into the brain of nude mice and injected either saline (control) or Dox intraperitoneally daily for 30 days. All mice treated with saline died with malignant glioma within 40 days, whereas the mice treated with Dox had better survival rates (median survival: GIC1, 38 [control] *vs* 59 [Dox] days; GIC2:36 [control] *vs* 69 [Dox] days) (Fig. 5B). In addition, we found that tumors in the Dox-treated mouse brains did not show necrosis or microvascular proliferation, essential features of GBM, although they still showed hypercellularity and infiltrated normal parenchyma, suggesting that Gli2ΔC overexpression reduced the malignancy of the cells (Fig. 5C).

The Gli → Cdc2 pathway is essential for GIC proliferation and tumorigenesis. Although there is increasing evidence that Gli transcription factors regulate many important factors in both NSC and cancer cells,[21,22] it has not been clear which of Gli's downstream factors are important for GIC proliferation. We were interested in the Gli-downstream factors Sox2, Bmi1, N-myc and Cdc2 as they play essential roles in both NSC and human glioma,[16,23–27] and we began by examining their expression in human GBM and GIC lines by RT-PCR. We found that human primary GBM samples and GIC lines express all of these factors (Fig. S2A). In addition, immunolabeling confirmed that Gli2, Sox2, Bmi1, N-myc and Cdc2 were present in all four GBM tissues (Fig. S2B) and in GIC xenografts (Fig. 2B and Fig. S2C), although the tissues also contained marker-negative cells.

To examine the functions of these candidate factors in GIC lines, we constructed shRNA expression vectors that knocked down each factor (Fig. S3), transfected them into the GIC lines, and examined the cell proliferation by MTT assay. We found that Cdc2 knockdown inhibited the proliferation of both GIC lines, but knockdown of other factors had little effect on

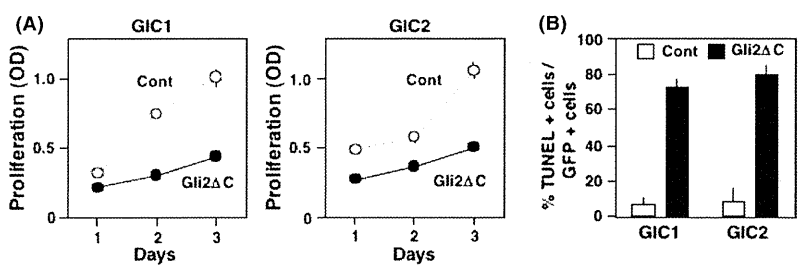

Fig. 4. Overexpressed Gli2ΔC induces cell cycle arrest and cell death in glioma-initiating cells (GIC). (A) GIC1 and GIC2 cells were transfected with either a control vector (open circles) or a Gli2ΔC expression vector (closed circles), and their proliferation was examined by MTT assay. (B) A TUNEL assay was performed on Gli2ΔC-expressing GIC1 and GIC2 cells.

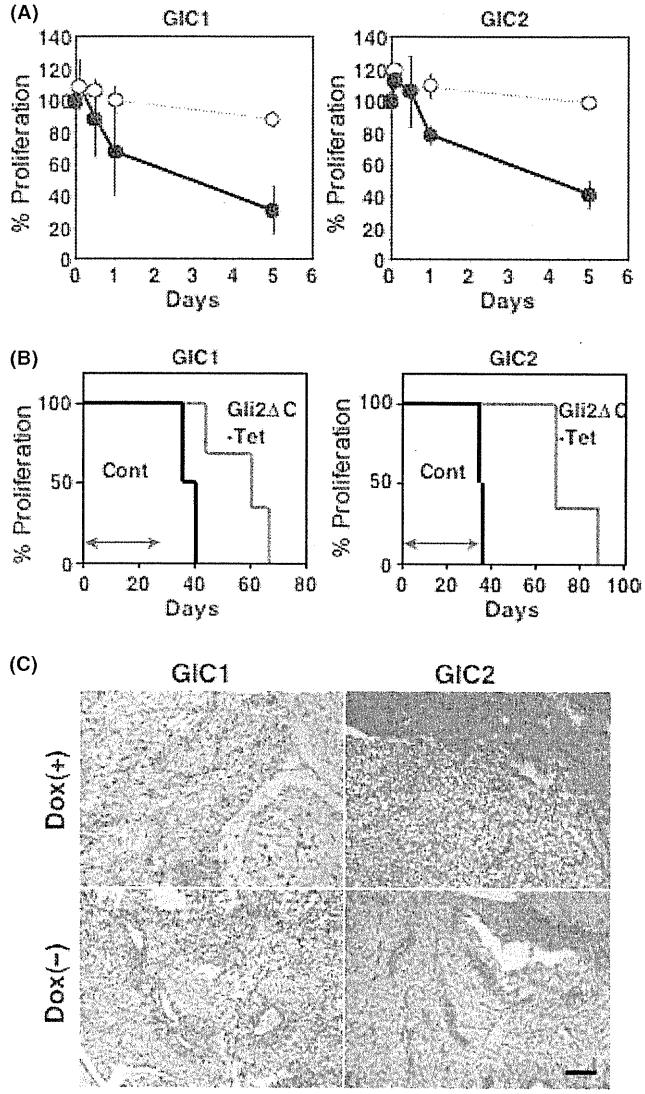

Fig. 5. Gli2ΔC overexpression inhibits glioma-initiating cell (GIC) tumorigenesis *in vivo*. (A) Proliferation of Tet-inducible Gli2ΔC-bearing GIC (closed circles) and control GIC (open circles) after Doxycycline (Dox) treatment was examined by MTT assay. (B) Survival curve of mice in which 10^3 control GIC (black line) or Tet-inducible Gli2ΔC-bearing GIC (red line) were transplanted. (C) Tumors formed from GIC, stained with hematoxylin–eosin in the presence (upper panels) or absence (lower panels) of Dox. Scale bar, 100 μm.

proliferation (Fig. 6), even though it inhibited NSC marker expression (data not shown). As it was shown that inhibition of Sox2 or Bmi1 resulted in impaired proliferation of GIC,[28–30] we further examined whether Sox2 and Bmi1 are generally essential for GIC proliferation. We cultured four tumorigenic GBM cell lines, U251, T98G, U118 and C6, in the NSC medium to enrich for GIC and examined the expression of *sox2*, *bmi1* and *cdc2* in the cells. We found that all cells express *cdc2*, whereas *bmi1* expression was at an undetectable level in these cells. In addition, *sox2* was expressed in U251 and C6 but not in the others (Fig. S4). Together with the immunolabeling data showing that GBM consists of both these marker-positive and -negative cells (Fig. 2B and Fig. S2B), this suggests that all GIC might not express Bmi1 and Sox2. Thus, these data indicate that the Gli downstream factor Cdc2 is essential for GIC proliferation.

Discussion

In the present study we established two human GIC lines, GIC1 and GIC2, from AO and GBM, respectively. Both GIC lines not only retained characteristics of NSC, but also formed malignant glioma with their original pathological features when transplanted *in vivo*, suggesting that they were enriched with CIC. Although GIC1 and GIC2 showed similar characteristics, we found in a parallel experiment that tumorigenesis of GIC1 was prevented by a combination of Cox2 and epidermal growth factor receptor (EGFR) signaling inhibitors, whereas that of GIC2 was not.[31] There are some possible explanations for this result. First, EGFR signaling is known to be involved in the proliferation and tumorigenesis of oligodendrocyte precursor cells.[32,33] Second, we found that GIC1 expressed EGFRvIII, which was shown by Mellinghoff *et al.*[34] to cause "pathway addiction" of the tumor cells. Third, the accumulation of Cox2-expressing astrocytes is more often observed in high-grade oligodendroglioma than in GBM.[35,36] Thus, these findings suggest that the therapeutic targets for malignant glioma are different according to the cell-of-origin of the GIC.

Hh signaling inhibitors blocked CIC proliferation, whereas either WIF or a γ-secretase inhibitor had little effect, suggesting that the Hh signaling pathway is crucial for GIC proliferation. Since many papers have shown that inhibitors of Notch or Wnt signaling block cancer cell proliferation, the inhibitors used in the present study might not have effectively prevented these pathways, or alternative pathways such as LIF and transforming growth factor might directly activate functional molecules in the Notch and Wnt signaling pathways in GIC lines, as shown previously.[37,38] Therefore, the question of whether Notch and Wnt signaling pathways are involved in GIC proliferation and maintenance still needs to be investigated further.

Our findings clearly indicate that the Hh/Gli signaling pathway is essential for gliomagenesis, as both Gli2ΔC overexpression and Hh inhibitors inhibited proliferation in these GIC lines. These findings suggest that inactivating the Hh/Gli pathway using RNAi or small chemical inhibitors is a potential therapeutic strategy. In addition, because in the absence of Hh both Gli2 and Gli3 are processed at their C-terminus and converted to dominant-negative regulators that block all Gli transcription factor functions,[39,40] it is of interest to determine which protease is involved in this processing and evaluate it as a potential therapeutic target.

The Hh/Gli signaling pathway is essential for the maintenance and proliferation of both NSC and brain tumor cells.[41] Indeed, Gli2ΔC overexpression induces cell cycle arrest and apoptosis not only in GIC (the current study) and in a C6 rat glioma cell line (data not shown), but also in NSC,[16] indicating the importance of finding drugs that kill GIC but not NSC. This also raises the question of whether GIC hijack the Hh/Gli signaling network in the process of transforming from non-NSC. Alternatively, NSC, as the glioma cell-of-origin, might transform into GIC. Both hypotheses seem to be true, as we have successfully induced GIC from both NSC and oligodendrocyte precursor cells when the cells lost p53 and expressed oncogenic H-Ras.[31]

Among the potential Gli target factors Bmi1, N-myc, Sox2 and Cdc2, we found Cdc2 to be indispensable for GIC proliferation. This is consistent with a previous finding that inhibiting Cdc2 induces cell cycle arrest and apoptosis at the G2/M phase in glioma cells.[42] Because Cdc2 is a critical regulator for the G2/M transition of every proliferating cell, it cannot serve as a direct target for therapy. However, the mechanism by which Gli regulates Cdc2 expression involves many transcription factors, including E2F and CREB, and that mechanism might be a therapeutic target. The findings that knockdown of Bmi1 and Sox2 did not inhibit GIC proliferation and that human GBM cell lines, T98G and U118, expressed neither *bmi1* nor *sox2* suggest that

doi: 10.1111/j.1349-7006.2011.01943.x

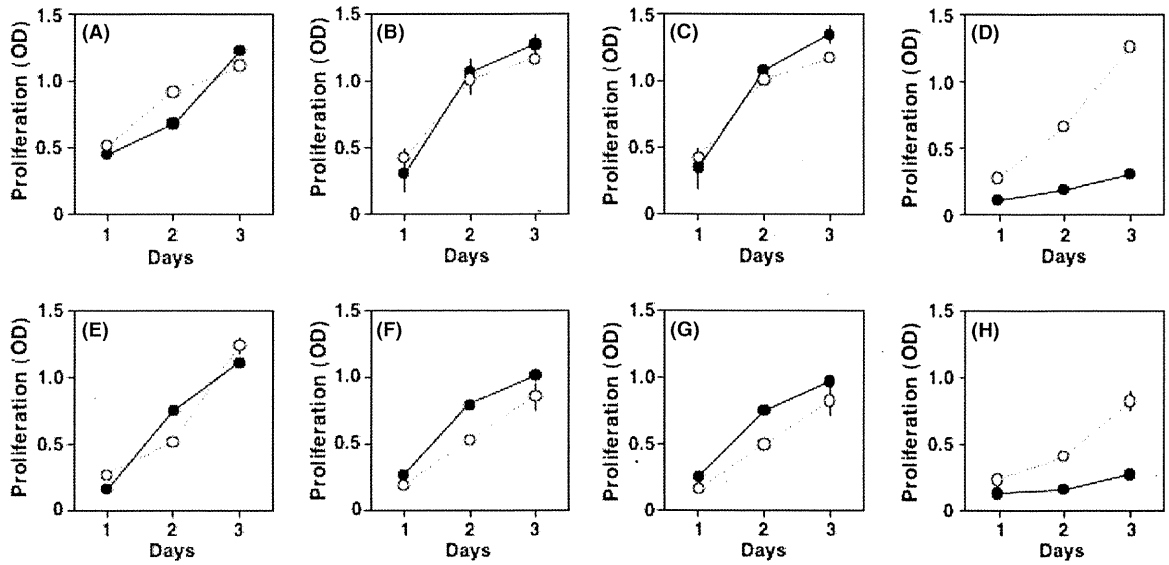

Fig. 6. Cdc2 is essential for the proliferation of glioma-initiating cell (GIC). MTT assays of GIC1 (A–D) and GIC2 (E–H) cell proliferation in the presence of either a control vector (open circles) or one of the following shRNA expression vectors (closed circles): Bmi1-shRNA (A,E), Sox2-shRNA (B,F), N-myc-shRNA (C,G) or Cdc2-shRNA (D,H).

Bmi1 and Sox2 might not be essential for GIC proliferation. Nonetheless, as Bmi1, N-myc or Sox2 knockdown prevented NSC marker expression in our GIC (data not shown), it will be interesting to investigate whether their knockdown blocks the tumorigenesis of our GIC lines.

Acknowledgments

The authors thank Maarten van Lohuizen (The Netherlands Cancer Institute, Amsterdam, The Netherlands) for the Bmi1 shRNA sequence, K. Ichimura and P. Collins (University of Cambridge, Cambridge, UK) for U251, T98G and U118 human GBM cell lines, and the members in Dr Kondo's Laboratory at the RIKEN CDB for their helpful comments and discussion. This work was supported in part by a Grant-In-Aid for Scientific Research on Priority Areas from the Ministry of Education, Culture, Sports, Science, and Technology of Japan to T.K.

Disclosure Statement

The authors have no conflict of interest.

References

1 Reya T, Morrison SJ, Clarke MF *et al.* Stem cells, cancer and cancer stem cells. *Nature* 2001; **414**: 105–11.
2 Singh K, Clarke ID, Hide T *et al.* Cancer stem cells in nervous system tumors. *Oncogene* 2004; **23**: 7267–73.
3 Kondo T. Brain cancer stem-like cells. *Eur J Cancer* 2006; **42**: 1237–42.
4 Vescovi AL, Galli R, Reynolds BA. Brain tumour stem cells. *Nat Rev Cancer* 2006; **6**: 425–36.
5 Pardal R, Clarke MF, Morisson SJ. Applying the principles of stem cell biology to cancer. *Nat Rev Cancer* 2003; **12**: 895–902.
6 Påhlman S, Stockhausen MT, Fredlund E, Axelson H. Notch signaling in neuroblastoma. *Semin Cancer Biol* 2004; **14**: 365–73.
7 Purow BW, Haque RM, Noel MW *et al.* Expression of Notch-1 and its ligands, Delta-like-1 and Jagged-1, is critical for glioma cell survival and proliferation. *Cancer Res* 2005; **65**: 2353–63.
8 Ruiz i Altaba A, Sánchez P, Dahmane N. Gli and hedgehog in cancer: tumours, embryos and stem cells. *Nat Rev Cancer* 2002; **2**: 361–72.
9 Pasca di Magliano M, Hebrok M. Hedgehog signalling in cancer formation and maintenance. *Nat Rev Cancer* 2003; **3**: 903–11.
10 Dahmane N, Sánchez P, Gitton Y *et al.* The Sonic Hedgehog-Gli pathway regulates dorsal brain growth and tumorigenesis. *Development* 2001; **128**: 5201–12.
11 Berman DM, Karhadkar SS, Hallahan AR *et al.* Medulloblastoma growth inhibition by hedgehog pathway blockade. *Science* 2002; **297**: 1559–61.
12 Chenn A, Walsh CA. Regulation of cerebral cortical size by control of cell cycle exit in neural precursors. *Science* 2002; **297**: 365–9.
13 Yu JM, Jun ES, Jung JS *et al.* Role of Wnt 5a in the proliferation of human glioblastoma cells. *Cancer Lett* 2007; **257**: 172–81.
14 Pu P, Zhang Z, Kang C *et al.* Downregulation of Wnt2 and beta-catenin by siRNA suppresses malignant glioma cell growth. *Cancer Gene Ther* 2009; **16**: 351–61.
15 Hide T, Takezaki T, Nakatani Y, Nakamura H, Kuratsu J, Kondo T. Sox11 prevents tumorigenesis of glioma-initiating cells by inducing neuronal differentiation. *Cancer Res* 2009; **69**: 7953–9.
16 Takanaga H, Tsuchida-Straeten N, Nishide K *et al.* Gli2 is a novel regulator of sox2 expression in telencephalic neuroepithelial cells. *Stem Cells* 2009; **27**: 165–74.
17 Kondo T, Setoguchi T, Taga T. Persistence of a small subpopulation of cancer stem-like cells in the C6 glioma cell line. *Proc Natl Acad Sci USA* 2004; **101**: 781–6.
18 Singh SK, Clarke ID, Terasaki M *et al.* Identification of a cancer stem cell in human brain tumors. *Cancer Res* 2003; **63**: 5821–8.
19 Yuan X, Curtin J, Xiong Y *et al.* Isolation of cancer stem cells from adult glioblastoma multiforme. *Oncogene* 2004; **23**: 9392–400.
20 Hsieh J, Aimone JB, Kaspar BK, Kuwabara T, Nakashima K, Gage FH. IGF-I instructs multipotent adult neural progenitor cells to become oligodendrocytes. *J Cell Biol* 2004; **164**: 111–22.
21 Stecca B, Ruiz i Altaba A. A GLI1-p53 inhibitory loop controls neural stem cell and tumour cell numbers. *EMBO J* 2009; **28**: 663–76.
22 Po A, Ferretti E, Miele E *et al.* Hedgehog controls neural stem cells through p53-independent regulation of Nanog. *EMBO J* 2010; **29**: 2646–58.
23 Regl G, Kasper M, Schnidar H *et al.* The zinc-finger transcription factor GLI2 antagonizes contact inhibition and differentiation of human epidermal cells. *Oncogene* 2004; **23**: 1263–74.
24 Liu S, Dontu G, Mantle ID *et al.* Hedgehog signaling and Bmi-1 regulate self-renewal of normal and malignant human mammary stem cells. *Cancer Res* 2006; **66**: 6063–71.
25 Schmitz M, Temme A, Senner V *et al.* Identification of SOX2 as a novel glioma-associated antigen and potential target for T cell-based immunotherapy. *Br J Cancer* 2007; **96**: 1293–301.
26 Katoh Y, Katoh M. Hedgehog target genes: mechanisms of carcinogenesis induced by aberrant hedgehog signaling activation. *Curr Mol Med* 2009; **9**: 873–86.

27 Wey A, Cerdeno VM, Pleasure D, Knoepfler PS. c- and N-myc regulate neural precursor cell fate, cell cycle, and metabolism to direct cerebellar development. *Cerebellum* 2010; **9**: 537–47.
28 Wiederschain D, Chen L, Johnson B *et al.* Contribution of polycomb homologues Bmi-1 and Mel-18 to medulloblastoma pathogenesis. *Mol Cell Biol* 2007; **27**: 4968–79.
29 Dovey JS, Zacharek SJ, Kim CF, Lees JA. Bmi1 is critical for lung tumorigenesis and bronchioalveolar stem cell expansion. *Proc Natl Acad Sci USA* 2008; **105**: 11857–62.
30 Chen Y, Shi L, Zhang L *et al.* The molecular mechanism governing the oncogenic potential of SOX2 in breast cancer. *J Biol Chem* 2008; **283**: 17969–78.
31 Hide T, Takezaki T, Nakatani Y, Nakamura H, Kuratsu J, Kondo T. Combination of a Ptgs2 inhibitor and an EGFR-signaling inhibitor prevents tumorigenesis of oligodendrocyte-lineage derived glioma-initiating cells. *Stem Cells* 2011; **29**: 590–9.
32 Aguirre A, Dupree JL, Mangin JM, Gallo V. A functional role for EGFR signaling in myelination and remyelination. *Nat Neurosci* 2007; **10**: 990–1002.
33 Ivkovic S, Canoll P, Goldman JE. Constitutive EGFR signaling in oligodendrocyte progenitors leads to diffuse hyperplasia in postnatal white matter. *J Neurosci* 2008; **28**: 914–22.
34 Mellinghoff IK, Wang MY, Vivanco I *et al.* Molecular determinants of the response of glioblastomas to EGFR kinase inhibitors. *N Engl J Med* 2005; **353**: 2012–24.
35 Deininger MH, Meyermann R, Trautmann K *et al.* Cyclooxygenase (COX)-1 expressing macrophages/microglial cells and COX-2 expressing astrocytes accumulate during oligodendroglioma progression. *Brain Res* 2000; **885**: 111–6.
36 Temel SG, Kahveci Z. Cyclooxygenase-2 expression in astrocytes and microglia in human oligodendroglioma and astrocytoma. *J Mol Histol* 2009; **40**: 369–77.
37 Caraci F, Gili E, Calafiore M *et al.* TGF-beta1 targets the GSK-3beta/beta-catenin pathway via ERK activation in the transition of human lung fibroblasts into myofibroblasts. *Pharmacol Res* 2008; **57**: 274–82.
38 Cao F, Hata R, Zhu P, Nakashiro K, Sakanaka M. Conditional deletion of Stat3 promotes neurogenesis and inhibits astrogliogenesis in neural stem cells. *Biochem Biophys Res Commun* 2010; **394**: 843–7.
39 Ruiz i Altaba A. Gli proteins encode context-dependent positive and negative functions: implications for development and disease. *Development* 1999; **126**: 3205–16.
40 Sasaki H, Nishizaki Y, Hui C, Nakafuku M, Kondoh H. Regulation of Gli2 and Gli3 activities by an amino-terminal repression domain: implication of Gli2 and Gli3 as primary mediators of Shh signaling. *Development* 1999; **126**: 3915–24.
41 Stecca B, Ruiz i Altaba A. Brain as a paradigm of organ growth: Hedgehog-Gli signaling in neural stem cells and brain tumors. *J Neurobiol* 2005; **15**: 476–90.
42 Chen H, Huang Q, Dong J, Zhai DZ, Wang AD, Lan Q. Overexpression of CDC2/CyclinB1 in gliomas, and CDC2 depletion inhibits proliferation of human glioma cells *in vitro* and *in vivo*. *BMC Cancer* 2008; **8**: 29.

Supporting Information

Additional Supporting Information may be found in the online version of this article:

Fig. S1. Effects of Hh inhibitors on GIC proliferation.

Fig. S2. Gli2, Sox2, Bmi1, N-myc and Cdc2 expression in human GBM and GIC.

Fig. S3. Knockdown efficiency of shRNA.

Fig. S4. Expression of *sox2*, *bmi1* and *cdc2* in GBM cell lines.

Table S1. List of primer sequences for RT-PCR.

Table S2. List of primer sequences for cDNA cloning.

Data S1. Materials and methods.

Please note: Wiley-Blackwell are not responsible for the content or functionality of any supporting materials supplied by the authors. Any queries (other than missing material) should be directed to the corresponding author for the article.

doi: 10.1111/j.1349-7006.2011.01943.x

Ann Nucl Med (2011) 25:432–438
DOI 10.1007/s12149-011-0483-1

ORIGINAL ARTICLE

Does adding FDG-PET to MRI improve the differentiation between primary cerebral lymphoma and glioblastoma? Observer performance study

Keishi Makino · Toshinori Hirai · Hideo Nakamura · Ryuji Murakami · Mika Kitajima · Yoshinori Shigematsu · Rumi Nakashima · Shinya Shiraishi · Hiroyuki Uetani · Koya Iwashita · Masuma Akter · Yasuyuki Yamashita · Jun-ichi Kuratsu

Received: 17 January 2011 / Accepted: 23 February 2011 / Published online: 16 March 2011

Abstract
Objective It is sometimes difficult to distinguish between primary central nervous system lymphomas (PCNSL) and glioblastoma multiforme (GBM). The aim of this study was to investigate whether the addition of ^{18}F-2-fluoro-2-deoxy-D-glucose positron emission tomography ([^{18}F]FDG-PET) and apparent diffusion coefficients (ADC) to conventional MRI improves diagnostic accuracy for distinguishing between PCNSL and GBM with similar MRI findings.
Methods We used conventional- and diffusion-weighted MRI and FDG-PET scans of 21 patients with histologically confirmed brain tumors exhibiting similar MRI findings (PCNSL, $n = 14$, GBM, $n = 7$) in our observer performance study that consisted of 3 interpretation sessions. ADC and maximum standard uptake values (SUV_{max}) of the tumors were calculated. Three radiologists first interpreted conventional MRI (1st session), then they read images to which the ADC value had been added (2nd session), and finally they interpreted images supplemented with SUV_{max} (3rd session). Observer performance was evaluated using κ statistic and receiver operating characteristics analyses.
Results The addition of ADC values to conventional MRI failed to improve the differentiation between PCNSL and GBM. The addition of SUV_{max} at the third session improved the diagnostic accuracy of all 3 readers and resulted in higher interobserver agreement; mean accuracy was 95% (range 93–100%). In one observer the accuracy of tumor differentiation was significantly improved at the third compared to the second session ($p = 0.017$).
Conclusions In a selected group of PCNSL and GBM with similar MRI findings, the addition of quantitative FDG-PET to MRI may improve their differentiation. ADC measurement did not allow further discrimination.

Keywords Brain tumors · PET · MRI

K. Makino and T. Hirai have contributed equally to this study.

K. Makino · H. Nakamura · J. Kuratsu
Department of Neurosurgery,
Graduate School of Medical Sciences,
Kumamoto University, Kumamoto, Japan

T. Hirai (✉) · M. Kitajima · Y. Shigematsu · S. Shiraishi · H. Uetani · K. Iwashita · M. Akter · Y. Yamashita
Department of Diagnostic Radiology,
Graduate School of Medical Sciences,
Kumamoto University, 1-1-1 Honjo,
Kumamoto 860-8556, Japan
e-mail: t-hirai@kumamoto-u.ac.jp

R. Murakami
Department of Radiation Oncology,
Graduate School of Medical Sciences,
Kumamoto University, Kumamoto, Japan

R. Nakashima
Japanese Red Cross Kumamoto Health Care Center,
Kumamoto, Japan

Introduction

Primary central nervous system lymphomas (PCNSL) are extranodal malignant tumors that arise in the brain, spinal cord, leptomeninges, or eyes; they account for less than 5% of all primary CNS tumors. As the incidence of PCNSL has increased over the last two decades all over the world [1–3], there is a need to differentiate between PCNSL and glioblastoma multiforme (GBM), the most common primary brain tumor in adults. For the selection of

appropriate treatment strategies, the accurate preoperative differentiation between PCNSL and GBM is imperative. For example, if the tumor is highly suspected of being PCNSL, stereotactic biopsy is usually recommended to confirm the diagnosis. If the tumor is highly suspected of being GBM, craniotomy would be chosen. Chemotherapy regimens are different for the two tumors.

It is often possible to differentiate between PCNSL and GBM on conventional MR images (MRI) alone. However, it can be difficult to distinguish between these tumors, especially when the PCNSL lesion is solitary and heterogeneously enhanced [4–6] or when the GBM lesion is homogeneously enhanced [7, 8]. Under these conditions additional imaging methods may be needed to improve diagnostic accuracy. Apparent diffusion coefficient (ADC) measurements in the tumor may be useful for the differentiation between PCNSL and high-grade glioma [9–12]. ^{18}F-2-fluoro-2-deoxy-D-glucose positron emission tomography (FDG-PET) has also been reported as a useful tool for differentiating PCNSL from high-grade glioma [13].

To our knowledge, there are no published data on the effect of adding ADC and FDG-PET to conventional MRI for the differentiation between PCNSL and GBM exhibiting similar MRI findings. Therefore, we studied whether the addition of ADC and FDG-PET to conventional MRI studies improves the diagnostic performance of radiologists charged with differentiating between PCNSL and GBM with similar MRI findings.

Materials and methods

Patients

Inclusion criteria for the observer performance study were (a) a PCNSL or GBM diagnosis histologically confirmed by biopsy or open surgery, (b) a solitary tumor with heterogeneous enhancement on conventional MRI for PCNSL, (c) a tumor with relatively homogeneous enhancement on conventional MRI for GBM, (d) no apparent body lesions on FDG-PET, (e) the availability for review of whole series of preoperative FDG-PET and conventional MR imaging data including ADC maps, (f) no corticosteroid and/or radiation therapy prior to PET and MRI study, (g) absence of diabetes mellitus, immunosuppression, or human immunodeficiency virus infection, and (h) an interval of 10 days or less between FDG-PET- and MRI studies. The presence of 2 or more enhanced lesions within a region of T2 prolongation was considered to represent a solitary lesion. Since GBM and PCNSL with typical MRI findings can be easily differentiated on conventional MRI scans, we chose tumors with following MRI findings: GBM with relatively homogeneous enhancement and PCNSL with a solitary mass and heterogeneous enhancement.

One experienced neuroradiologist (T.H.) and one experienced neurosurgeon (K.M.) evaluated the cases together. Between January 2003 and December 2008, these criteria were satisfied by 21 patients (13 males, 8 females, age range 37–81 years, mean 67 years); 14 presented with PCNSL and the other 7 with GBM. The total number of cases with GBM and PCNSL during the period were 123 and 60, respectively. The rate of the selected case with GBM was 7/123 (5.7%); that with PCNSL was 14/60 (23.3%).

The main location of PCNSL was the parietal lobe in 3 patients, the basal ganglia in 3, the thalamus in 3, the corpus callosum in 2, and the frontal and parietal lobes and cerebellum in one each; that of GBM was the temporal lobe in 3, and the basal ganglia, thalamus, corpus callosum, and frontal lobe in one each.

MRI

MRI scans were obtained on a 1.5-T superconducting system (Magnetom Vision; Siemens, Erlangen, Germany) until December 2006, thereafter we used a 3.0-T instrument (Magnetom Trio; Siemens). Conventional MRI and diffusion-weighted images (DWI) were acquired during the same procedure. For conventional MRI study we used a sagittal T1-weighted localizing sequence and axial T1-weighted, fast spin-echo T2-weighted, fluid-attenuated inversion-recovery (FLAIR), and triplanar contrast-enhanced T1-weighted sequences. For contrast-enhanced studies we intravenously (i.v.) injected gadopentetate dimeglumine (0.1 mmol/kg body weight; Magnevist; Bayer-Schering, Berlin, Germany). The parameters for T1- and T2-weighted and FLAIR sequences were: section thickness 5 mm, section gap 1 mm, matrix size 256 × 256–512, field of view (FOV) 220 × 220 mm.

DWI at the 2 MRI units was performed in the axial plane by using a single-shot echo planar imaging sequence; the parameters were: TR ms/TE ms 12000/100 for 1.5T and 3600/81 for 3T, diffusion gradient encoding in 3 orthogonal directions $b = 0$ and 1000 s/mm^2, FOV 230 × 230 mm, matrix size 128 × 128 pixels, section thickness 5 mm, section gap 1 mm. DWI was performed before contrast-enhanced T1-weighted imaging.

The ADC values were calculated as: $\mathrm{ADC} = -[\ln(S/S_0)]/b$, where S is the signal intensity (SI) of the region of interest (ROI) on 3 orthogonally oriented DWIs or diffusion trace images, S_0 is the SI of the ROI on reference T2-weighted images, and b is the gradient b factor with a value of 1000 s/mm^2. ADC maps were calculated on a pixel-by-pixel basis.

FDG-PET

For FDG-PET studies we used a PET/CT scanner (Discovery ST; GE Healthcare, Milwaukee, WI) for all 21 patients. All PET studies were performed as head- and full head-to-thigh scans to evaluate both the brain tumor and other body lesions. After a fast, lasting a minimum of 5 h, head FDG-PET scans were obtained 50 min after the i.v. injection of 3.7 MBq/kg of FDG; this was followed by head-to-thigh scanning. The reconstructed images had a slice thickness of 2 mm and a matrix of 128 × 128 for the head and of 4 mm and 144 × 144 for the body. Before PET we acquired unenhanced CT scans from the head to the upper thigh; the settings were: transverse 3.75-mm section thickness, 120 kVp, 108 mA, and 16.8-mm table speed. Images were reconstructed by ordered-subset expectation maximization two-dimensional interactive reconstruction; CT images were used to produce attenuation correction values for PET emission reconstruction and fused PET/CT presentation. Reconstruction images were converted to standard uptake value (SUV) images using the equation: SUV = activity at a pixel (kBq/cm^3)/injection dose (MBq)/weight (kg).

Image analysis

PET/CT images were analyzed using PET/CT software (Xeleris, GE Healthcare). Several circular ROIs were placed over the tumor using information obtained by an experienced radiologist (R.N.) from contrast-enhanced MRI studies. Slices displaying maximum tumor activity were selected. Necrotic or cystic tumor portions on contrast-enhanced MRI scans were excluded from the ROI. The ROI area over tumors was at least 1.5 cm^2. We used maximum SUV (SUV_{max}) among the SUVs obtained [13].

To assess the brain tumors based on imaging-, surgical-, and histopathologic data, one neuroradiologist (T.H.) and one neurosurgeon (K.M.) with 18 and 13 years of experience in brain MRI, respectively, consensually evaluated the entire series of MRI scans on a PACS workstation. They were cognizant of clinical and histopathologic data. They also consensually identified solid tumor components with contrast enhancement on conventional MRI scans and ADC maps. They carefully inspected the conventional MR images; ROIs were manually drawn on ADC maps in areas corresponding to the enhancing portion of the lesions. According to the previous reports [9, 11, 12], ROIs with diameter ranges from 0.7 to 1.2 cm were placed centrally within the largest solid-enhancing area of the tumor to avoid volume averaging with cysts and necrotic areas that might have influenced ADC values.

Observer performance study

Three radiologists (Y.S., R.M., M.K.) participated in the observer performance study. Each reader had 15–18 years of experience (mean 17 years) interpreting brain MRI. They were blinded to all clinical data including pathologic findings, but they were informed that the tumor was either PCNSL or GBM. They used a 5-point confidence scale; no limit was imposed on the reading time.

Each case was subjected to 3 interpretation sessions using a PACS workstation and a 21-in. monitor. At the first session the readers were provided with only the conventional MRI scan to evaluate morphologic features, SI, and lesional contrast enhancement patterns [4–7]. Axial views of pre and postcontrast T1-weighted images, and T2-weighted and FLAIR images were evaluated. Each reader assessed the lesions using a 5-point confidence scale where 1 = definitely PCNSL, 2 = probably PCNSL, 3 = equivocal, 4 = probably GBM, and 5 = definitely GBM.

After the first interpretation, each reader performed a second interpretation where ADC maps and ADC values in the lesion were shown. Each reader was provided with the recommended optimal cutoff point for an ADC value and its accuracy, sensitivity, and specificity and re-assessed the lesion using the same 5-point confidence scale.

For the third interpretation, readers were shown the PET images and SUV_{max} measured in the lesion. The recommended optimal cutoff point for SUV_{max} and accuracy, sensitivity, and specificity data were provided and each reader re-assessed the lesion using the same 5-point confidence scale. After completing the third interpretation of individual cases, the readers proceeded to the first interpretation of the next case.

Statistical analyses

For each tumor type the mean and standard deviation (SD) of the ADC and SUV_{max} were calculated. These values of the solid-enhancing areas of the PCNSL and GBM were compared using the unpaired t test. ROC curves were generated from the ADC values and SUV_{max} of the 21 cases included in this study. Accuracy (A_z), represented by the area under the ROC curve, and the cutoff point, sensitivity and specificity of the ADC and SUV_{max} were calculated and recorded. These data were used in the observer performance study. The difference in accuracy between the ADC alone and the SUV_{max} alone was evaluated for statistical significance by pairwise comparison of the ROC curves [14].

In each observer performance study, ROC analysis was performed using the 5-point confidence scale. Accuracy, represented by the area under the ROC curve, sensitivity,

and specificity of each reader's interpretation, with corresponding standard errors and variance, were calculated. Changes in each reader's accuracy between the first and second interpretation session were evaluated for statistical significance by using pairwise comparison of the ROC curves [14].

Interobserver differences were assessed to establish the reliability of the interpretations. The degree of the interobserver difference between combinations of 2 readers was calculated with the chance-corrected κ statistic. κ statistic results were categorized as follows: a κ value greater than or equal to 0 but less than or equal to 0.20 = slight agreement, a κ value greater than or equal to 0.21 but less than or equal to 0.40 = fair agreement, a κ value greater than or equal to 0.41 but less than or equal to 0.60 = moderate agreement, a κ value greater than or equal to 0.61 but less than or equal to 0.80 = substantial agreement, a κ value greater than or equal to 0.81 but less than or equal to 1.00 = excellent agreement [15].

All statistical analyses were performed with standard statistical methods using a computer software package (MedCalc; MediSoftware, Mariakerke, Belgium). Differences of $p < 0.05$ were considered significant.

Results

ROC analysis of ADC and SUV_{max}

The distribution of the ADC values and SUV_{max} for PCNSL and GBM is shown in Fig. 1. The mean ± SD of the ADC values was 0.81 ± 0.21 × $10^{-3}mm^2/s$ (range 0.48–1.21 × $10^{-3}mm^2/s$) for PCNSL and 0.94 ± 0.24 × $10^{-3}mm^2/s$ (range 0.69–1.39 × $10^{-3}mm^2/s$) for GBM; the difference was not statistically significant. For SUV_{max} they were 16.76 ± 7.19 (range 7.9–30.5) for PCNSL and 8.24 ± 3.05 (range 4.0–12) for GBM. The mean SUV_{max} of PCNSL was significantly higher than of GBM ($p < 0.01$).

The ROC curve generated from ADC values and SUV_{max} in the 21 lesions is shown in Fig. 2. The optimal cutoff point for the ADC and SUV_{max} was 0.8 × $10^{-3}mm^2/s$ and 12, respectively. An ADC of 0.8 × $10^{-3}mm^2/s$ or greater suggested GBM, whereas an ADC of less than 0.8 × $10^{-3}mm^2/s$ suggested PCNSL. The accuracy (A_z) of the ADC alone for lesion differentiation with a cutoff point of 0.8 × $10^{-3}mm^2/s$ was 0.68; sensitivity was 71.4 and specificity 64.3%. A SUV_{max} of 12 or greater suggested PCNSL; a value less than 12 suggested GBM. The accuracy (A_z) of SUV_{max} alone for lesion differentiation with a cutoff point of 12 was 0.86; sensitivity was 100%, and specificity was 71.4%. There was no significant difference in the accuracy (A_z) between SUV_{max} and the ADC value ($p = 0.19$).

Observer performance study and interobserver agreement

As shown in Table 1, adding the ADC at the first interpretation session resulted in 2 readers achieving slightly higher accuracy in the discrimination between PCNSL and GBM; it was lower for the other reader. The mean accuracy for lesion differentiation was 74% (range 68–82%) at the first and 75% (range 61–89%) at the second session; the difference between the 2 sessions was not significant. Figure 3 shows the ROC curves generated from the probability of a PCNSL assignment by a representative reader.

The addition of SUV_{max} at the third interpretation session resulted in higher correct tumor type identification by all 3 readers (Table 1). The mean accuracy for tumor differentiation was 75% (range 61–89%) at the second and 95% (range 93–100%) at the third interpretation. One reader achieved significantly higher accuracy at the third compared to the second interpretation ($p = 0.017$).

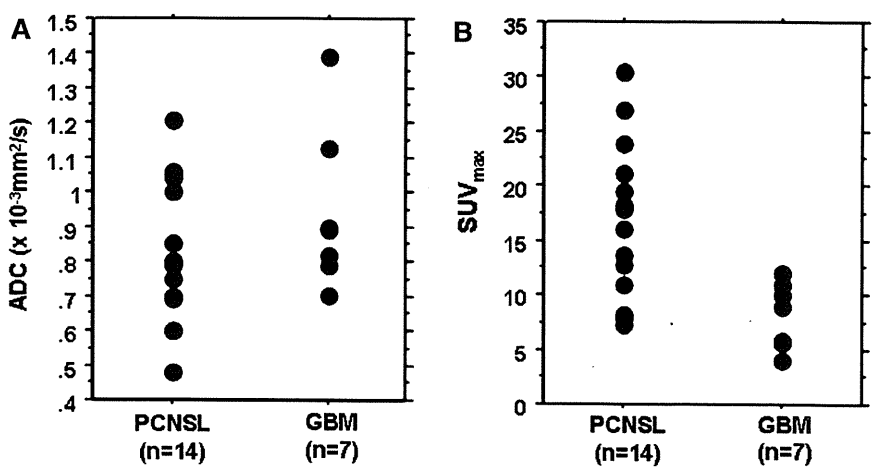

Fig. 1 Scatterplots of the ADC value (**a**) and SUV_{max} (**b**) measured in solid-enhancing PCNSL and GBM tumors. There was no significant difference between the mean ADC value of PCNSL and GBM. The mean SUV_{max} of PCNSL was significantly higher than of GBM ($p < 0.01$)

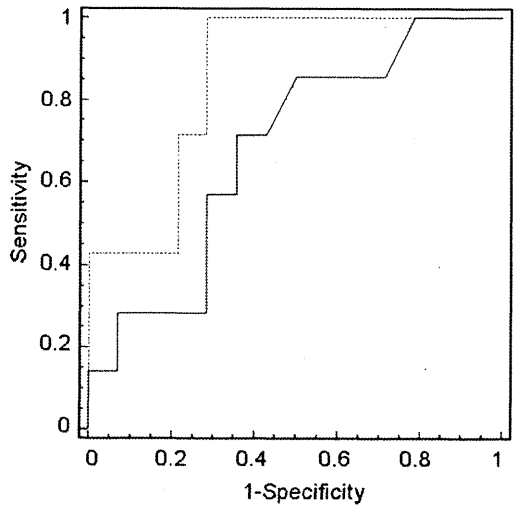

Fig. 2 ROC curve generated from the ADC value and SUV_{max} measured in 21 PCNSL and GBM lesions. *The solid line* represents the ROC curve generated from the lesional ADC values; the *dashed line* the ROC curve generated from the SUV_{max} of the lesions. With an ADC value cutoff point of $0.8 \times 10^{-3}mm^2/s$, accuracy (A_z) was 0.68, sensitivity was 71.4%, and specificity was 64.3%. With a SUV_{max} cutoff point of 12, A_z was 86%, sensitivity was 100%, and specificity was 71.4%. There was no significant difference in accuracy (A_z) between SUV_{max} and the ADC value ($p = 0.19$)

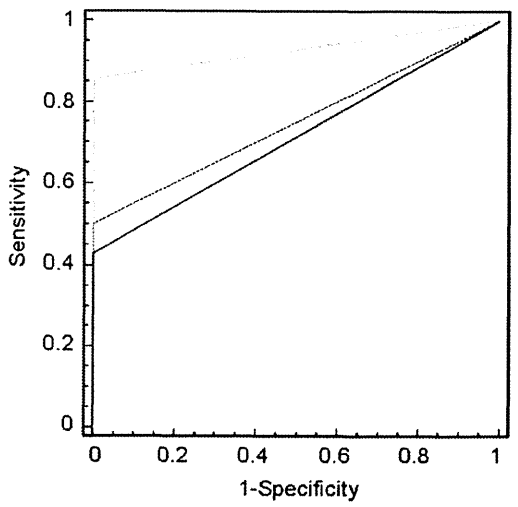

Fig. 3 ROC curves for one observer (reader 2) based on the probability of a PCNSL assignment. On each graph the *blue line* represents the ROC curve generated from the first interpretation session. It was based on morphologic features, the SI, and the lesional contrast enhancement pattern on conventional MRI scans. The *dashed brown line* represents the ROC curve generated from the second interpretation session; it is based on conventional MRI findings and the lesional ADC value. The *orange line* represents the ROC curve generated from the third interpretation session; it is based on conventional MRI findings, the ADC value, and SUV_{max} of the lesion. Note that accuracy (expressed as the area under the ROC curve) of the third session that included SUV_{max} of the lesion (*orange line*) is improved compared to the first and second interpretation sessions (*blue* and *dashed brown lines*)

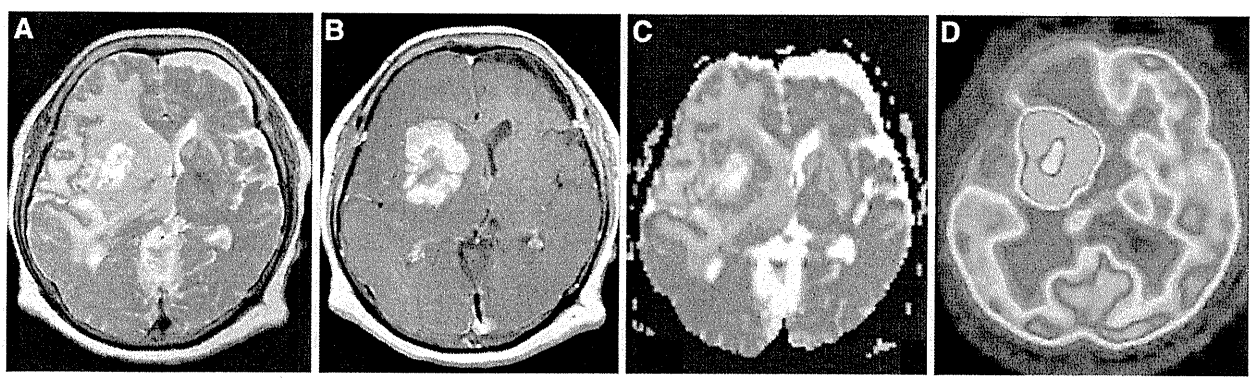

Fig. 4 A 75-year-old woman with PCNSL. **a** T2-weighted image demonstrating a heterogeneous hyperintense lesion (*arrows*) in the right basal ganglia and surrounding hyperintensity areas. **b** Contrast-enhanced T1-weighted image showing a ring-like enhanced lesion in the right basal ganglia. After evaluating the morphologic features, signal intensity, and contrast enhancement patterns of the lesion on conventional MRI, 2 of the 3 readers scored the lesion as probably GBM; the third recorded the finding as equivocal. **c** On the ADC map, the enhancing solid lesion is nearly isointense relative to the normal brain (*arrow*). The ADC value of the enhancing solid portion is $0.8 \times 10^{-3}mm^2/s$. After evaluating conventional MRI scans supplemented with the ADC value, 2 of 3 readers submitted a reading of probably GBM, the third considered the finding equivocal. **d** On FDG-PET images, the enhancing solid lesion exhibited a higher uptake than the normal cerebral cortices. SUV_{max} of the lesion is 21.1. After evaluating conventional MRI scans, ADC, and SUV_{max}, all 3 observers submitted a reading of probable PCNSL

The κ values indicating the confidence level among the 3 readers for image interpretation are shown in Table 2. The addition of ADC for the second interpretation resulted in lower interobserver agreement between all pairs of readers. The addition of SUV_{max} at the third interpretation session produced higher

Table 1 Accuracy of assigned probabilities of differentiating PCNSL from glioblastoma

Reader and interpretation	Accuracy of assigned probability		
	Value (%)	95% CI	*p* value
Reader 1			
Initial interpretation	82	0.59–0.95	
Second interpretation	89	0.68–0.98	0.50
Third interpretation	100	0.84–1.00	0.13
Reader 2			
Initial interpretation	71	0.48–0.89	
Second interpretation	75	0.52–0.91	0.77
Third interpretation	93	0.73–0.99	0.12
Reader 3			
Initial interpretation	68	0.44–0.86	
Second interpretation	61	0.37–0.81	0.66
Third interpretation	93	0.73–0.99	0.017

Initial interpretation was based on conventional MR imaging findings including the morphologic features, signal intensity and contrast enhancement patterns of the lesion. Second interpretation was based on conventional MR imaging findings and ADC value of the lesion. Third interpretation was based on conventional MR imaging findings, ADC value and SUV_{max} of the lesion. The change in each reader's accuracy between the initial and second interpretations and between the second and third interpretations was evaluated for statistical significance by using the pairwise comparison of ROC curves

Table 2 Interobserver agreement of assessment for tumor discrimination with a five-point confidence scale

Comparison	Initial interpretation	Second interpretation	Third interpretation
R1 versus R2	0.61	0.46	0.64
R1 versus R3	0.37	0.19	0.62
R2 versus R3	0.44	0.40	0.60

Data are κ value

R1 reader 1, *R2* reader 2, *R3* reader 3

interobserver agreement between all pairs of readers (Fig. 4; Table 2).

Discussion

Overall, adding the tumor ADC value to conventional MRI studies resulted in slightly higher accuracy and lower interobserver agreement with respect to tumor differentiation. In one observer the addition of the ADC value to conventional MRI scans lowered accuracy. This finding suggests that adding the tumor ADC to conventional MRI studies fails to offer a sufficient advantage over the use of morphologic features, SI, and lesional contrast enhancement patterns in the differentiation between PCNSL and GBM. Earlier studies [9–12] indicated that there are various ranges in the ADC value for PCNSL and GBM. The mean ADC values ranged from 0.63 to 0.87 $\times$ $10^{-3}mm^2/s$ for PCNSL and from 0.90 to 1.13 $\times$ $10^{-3}mm^2/s$ for GBM. The mean ADC values of PCNSL and GBM in our patients were similar to previously reported data, although the mean ADC values of PCNSL and GBM in our study were not significantly different.

On the other hand, the addition of the tumor SUV_{max} at the third interpretation session resulted in higher accuracy and interobserver agreement compared to assessments performed on conventional MRI supplemented with the ADC value. Overall, the addition of SUV_{max} improved reader accuracy by as much as 20%. More importantly, the reader with the highest accuracy (89%) at the second interpretation achieved improved accuracy after assessing the SUV_{max} data. This suggests that adding SUV_{max} to MRI provides useful additional information for the discrimination between PCNSL and GBM.

Although FDG-PET has been reported as a useful tool for differentiating PCNSL from high-grade glioma [13], the value of adding FDG-PET to conventional MRI for the differentiation of PCNSL and GBM has not been described. Kosaka et al. [13] identified SUV_{max} on FDG-PET as the most important parameter for distinguishing lymphomas from other brain tumors. They used a SUV_{max} of 15 as a cutoff for diagnosing CNS lymphoma and only one high-grade glioma (SUV_{max}, 18.8) returned a false-positive result. Based on their findings we used SUV_{max} on FDG-PET images in our study; the optimal cutoff point for SUV_{max} was 12. The accuracy of SUV_{max} alone for distinguishing PCNSL from GBM (cutoff point 12) was 86%; sensitivity was 100% and specificity was 71.4%. SUV measurements of brain tumors may be influenced by a wide variety of factors such as the plasma glucose level, steroid treatment, time after tracer injection, and previous irradiation [16, 17]. We carefully excluded patients with diabetes mellitus, steroid treatment, and/or previous irradiation.

As did others [4–7], we document here that conventional MRI studies are valuable for distinguishing PCNSL from GBM. Although difficult cases with similar MRI findings, i.e., GBM with relatively homogeneous enhancement and PCNSL with a solitary mass and heterogeneous enhancement, were included in our study, approximately 75% of lesions could be differentiated on conventional MRI alone. Based on our results, we recommend that FDG-PET be added in cases where it is difficult to differentiate between PCNSL and GBM on conventional MRI scans and ADC maps.

Our study has some limitations. First, we used two different MR units at 1.5T and 3T. Although the absolute

ADC values of the brain may vary at 1.5 and 3.0T, the difference of ADC value between 1.5-T and 3.0-T imagers from the same vendor was only 3–5% [18]. We measured ADC values of normal gray matter and white matter in the 21 patients performed by 1.5 or 3.0 T. The difference of ADC values of normal gray matter and white matter between 1.5- and 3.0-T imagers was within 5 and 4%, respectively. Therefore, we think that the variability in the absolute ADC values between these units in our study was an acceptable range. Second, our study design may have imposed bias. The observer performance study included 3 interpretation sessions per case: at the first session only conventional MRI were read, at the second session the ADC value was added to conventional MRI, and at the third, conventional MRI, the ADC value, and SUV_{max} were available for interpretation. As the ADC value was added at the second session, we were unable to evaluate the influence of only the addition of SUV_{max} to conventional MRI. In routine clinical practice, diffusion-weighted imaging including the ADC is widely used for assessing various pathologic conditions. Therefore, our second interpretation session that included the ADC value could be considered to reflect the interpretation of routine conventional MRI. Third, there is a difference between observer performance studies and the clinical environment. As we provided our observers with information on the two tumor types, their performance may have been affected. Because there were only two types, the answer to 50% of the questions would have been correct from the outset. Fourth, our study was retrospective and the study population was relatively small.

In conclusion, in a selected group of PCNSL and GBM with similar MRI findings, the addition of quantitative FDG-PET to MRI studies may improve the radiologists' ability to differentiate between PCNSL and GBM.

Conflict of interest The authors declare that they have no conflict of interest.

References

1. van der Sanden GA, Schouten LJ, van Dijck JA, van Andel JP, van der Maazen RW, Coebergh JW. Primary central nervous system lymphomas: incidence and survival in the Southern and Eastern Netherlands. Cancer. 2002;94:1548–56.
2. Olson JE, Janney CA, Rao RD, Cerhan JR, Kurtin PJ, Schiff D, et al. The continuing increase in the incidence of primary central nervous system non-Hodgkin lymphoma: a surveillance, epidemiology, and end results analysis. Cancer. 2002;95:1504–10.
3. Makino K, Nakamura H, Kino T, Takeshima H, Kuratsu J. Rising incidence of primary central nervous system lymphoma in Kumamoto, Japan. Surg Neurol. 2006;66:503–6.
4. Koeller KK, Smirniotopoulos JG, Jones RV. Primary central nervous system lymphoma: radiologic–pathologic correlation. Radiographics. 1997;17:1497–526.
5. Erdag N, Bhorade RM, Alberico RA, Yousuf N, Patel MR. Primary lymphoma of the central nervous system: typical and atypical CT and MR imaging appearances. AJR Am J Roentgenol. 2001;176:1319–26.
6. Coulon A, Lafitte F, Hoang-Xuan K, Martin-Duverneuil N, Mokhtari K, Blustajn J, et al. Radiographic findings in 37 cases of primary CNS lymphoma in immunocompetent patients. Eur Radiol. 2002;12:329–40.
7. Rees JH, Smirniotopoulos JG, Jones RV, Wong K. Glioblastoma multiforme: Radiologic-pathologic correlation. Radiographics. 1996;16:1413–38.
8. Toh CH, Chen YL, Hsieh TC, Jung SM, Wong HF, Ng SH. Glioblastoma multiforme with diffusion-weighted magnetic resonance imaging characteristics mimicking primary brain lymphoma. Case report. J Neurosurg. 2006;105:132–5.
9. Guo AC, Cummings TJ, Dash RC, Provenzale JM. Lymphomas and high-grade astrocytomas: comparison of water diffusibility and histologic characteristics. Radiology. 2002;224:177–83.
10. Yamasaki F, Kurisu K, Satoh K, Arita K, Sugiyama K, Ohtaki M, et al. Apparent diffusion coefficient of human brain tumors at MR imaging. Radiology. 2005;235:985–91.
11. Toh CH, Castillo M, Wong AM, Wei KC, Wong HF, Ng SH, et al. Primary cerebral lymphoma and glioblastoma multiforme: differences in diffusion characteristics evaluated with diffusion tensor imaging. AJNR Am J Neuroradiol. 2008;29:471–5.
12. Horger M, Fenchel M, Nägele T, Moehle R, Claussen CD, Beschorner R, et al. Water diffusivity: comparison of primary CNS lymphoma and astrocytic tumor infiltrating the corpus callosum. AJR Am J Roentgenol. 2009;193:1384–7.
13. Kosaka N, Tsuchida T, Uematsu H, Kimura H, Okazawa H, Itoh H. 18F-FDG PET of common enhancing malignant brain tumors. AJR Am J Roentgenol. 2008;190:W365–9.
14. Hanley JA, McNeil BJ. A method of comparing the areas under receiver operating characteristic curves derived from the same cases. Radiology. 1983;148:839–43.
15. Landis JR, Koch GG. The measurement of observer agreement for categorical data. Biometrics. 1977;33:159–74.
16. Rosenfeld SS, Hoffman JM, Coleman RE, Glantz MJ, Hanson MW, Schold SC. Studies of primary central nervous system lymphoma with fluorine-18-fluorodeoxyglucose positron emission tomography. J Nucl Med. 1992;33:532–6.
17. Hustinx R, Smith RJ, Benard F, Bhatnagar A, Alavi A. Can the standardized uptake value characterize primary brain tumors on FDG-PET? Eur J Nucl Med. 1999;26:1501–9.
18. Sasaki M, Yamada K, Watanabe Y, Matsui M, Ida M, Fujiwara S, et al. Variability in absolute apparent diffusion coefficient values across different platforms may be substantial: a multivendor, multi-institutional comparison study. Radiology. 2008;249:624–30.

J Neurooncol (2011) 101:495–504
DOI 10.1007/s11060-010-0276-8

CLINICAL STUDY – PATIENT STUDY

Early detection of venous thromboembolism in patients with neuroepithelial tumor: efficacy of screening with serum D-dimer measurements and Doppler ultrasonography

Tomohiro Kawaguchi · Toshihiro Kumabe · Masayuki Kanamori · Taigen Nakamura · Ryuta Saito · Yoji Yamashita · Yukihiko Sonoda · Mika Watanabe · Teiji Tominaga

Received: 8 February 2010 / Accepted: 16 June 2010 / Published online: 29 June 2010

Abstract The efficacy of combined serum D-dimer level measurement and Doppler ultrasonography of the lower extremity was investigated for screening of venous thromboembolism (VTE) in patients with neuroepithelial tumor. Eighty-one patients with neuroepithelial tumor were prospectively studied. All patients underwent measurement of serum D-dimer levels and Doppler ultrasonography of the lower extremity. The serum D-dimer level was measured every week, and Doppler ultrasonography was performed two and two weeks after surgery, then every two weeks until discharge, or every two weeks for patients who did not undergo surgery. If the serum D-dimer level increased over 10.0 μg/ml, Doppler ultrasonography or computed tomography was performed to detect VTE. VTE occurred in 12 (14.8%) patients (seven males and five females; age 34–75, mean 59.0 years). Only one patient was symptomatic, whereas 11 patients identified by the screening were without symptoms. Five patients were treated with anticoagulant therapy, one with prophylactic inferior vena cava filter placement with anticoagulant therapy, and the other six were closely followed up without medication. No patient died of pulmonary embolism. Serial Doppler ultrasonography showed thrombus regression or organization and no thrombus extension. The maximum serum D-dimer value was significantly higher in patients with VTE than in those without VTE (mean 14.5 vs. 3.46 μg/ml, $P < 0.001$). The D-dimer cutoff value of 5.4 μg/ml could be used to identify VTE with 83% sensitivity and 84% specificity. The combination of sequential serum D-dimer measurement and Doppler ultrasonography of the lower extremity is an efficient and non-invasive procedure for identifying asymptomatic VTE in patients with neuroepithelial tumor.

Keywords Venous thromboembolism · Glioma · D-dimer · Doppler ultrasonography · Pulmonary embolism

T. Kawaguchi · T. Kumabe (✉) · M. Kanamori · T. Nakamura · R. Saito · Y. Yamashita · Y. Sonoda · T. Tominaga
Department of Neurosurgery, Tohoku University Graduate School of Medicine, 1-1 Seiryo-machi, Aoba-ku, Sendai, Miyagi 980-8574, Japan
e-mail: kuma@nsg.med.tohoku.ac.jp

M. Watanabe
Department of Pathology, Tohoku University Hospital, Sendai, Miyagi, Japan

Introduction

Venous thromboembolism (VTE), including pulmonary embolism (PE) and deep vein thrombosis (DVT), is a high-risk complication of cancer with significant clinical consequences known since the 19th century [1–3]. VTE is a leading cause of death in cancer patients [4] and is associated with significantly worse survival [5, 6]. Brain tumor is associated with high incidences of VTE [7–9], and patients with glioma have the highest incidence of VTE of 7.5% and PE of 2.3% [8]. However, previous studies of the incidence of VTE or its association with glioma were retrospective and asymptomatic VTE was not carefully considered.

The clinical features and symptoms of DVT are mainly non-sensitive and non-specific, so diagnosis usually depends on imaging methods. Doppler ultrasonography is regarded as the standard method because of less invasiveness and higher sensitivity [10]. Doppler ultrasonography is performed optimally for diagnosis of symptomatic, proximal vein thrombosis [11–19]. The serum D-dimer